THE PENNSYLVANIA STATE UNIVERSITY
SCHREYER HONORS COLLEGE

DEPARTMENT OF MECHANICAL ENGINEERING

# Parametric Study of Shear Sleeves in Thick Composite Joints to Maximize Fatigue Life

LUKE JEFFERY
FALL 2024

A thesis
submitted in partial fulfillment
of the requirements
for a baccalaureate degree
in Mechanical Engineering
with honors in Mechanical Engineering

Reviewed and approved* by the following:

Dr. Matthew Lear
Assistant Research Professor of Engineering Science and Mechanics
Thesis Supervisor

Dr. Jean-Michel Mongeau
Assistant Professor of Mechanical Engineering
Honors Adviser

* Electronic approvals are on file.

# ABSTRACT

Thick composites are increasingly used across multiple industries such as aerospace, automotive, marine, construction and defense due to their high strength-to-weight ratio and customizable material properties. These industries typically create large, long-lasting structures that are bolted together, necessitating the maximation of fatigue life in structural joints. Promising studies have highlighted the potential of using bolt sleeves to improve fatigue life by creating interference fits within the composite without causing installation damage. This study investigates how bolt sleeve geometry, specifically interference and sleeve thickness, can be optimized to maximize fatigue life. The objectives are to establish a method for evaluating fatigue performance in shear sleeves within composite joints, conduct a parametric sweep exploration of sleeve geometry, and evaluate the effects of shear sleeve geometry to recommend optimal designs. A finite element (FE) submodel of a larger, complex bolted composite joint is employed to efficiently conduct the parametric study. Fatigue life is estimated with the Goodman relation to account for alternating and mean stresses in the sleeve. Results confirm that both interference and thickness impact fatigue life. Increasing thickness reduces both alternating and mean stresses, enhancing fatigue life. In contract, increasing interference has a more complex effect: at high applied loads, it may reduce alternating stress, but at a certain threshold, it raises mean stress enough to ultimately lower fatigue life. The findings suggest that the optimal shear sleeve geometry for improved fatigue life combines minimal interference with maximized thickness. By providing practical design recommendations and identifying avenues for future research, this work contributes to improving joint fatigue performance in bolted thick composite joints.

# TABLE OF CONTENTS

## LIST OF FIGURES

## LIST OF TABLES

## ACKNOWLEDGEMENTS

I would like to express my deep gratitude to the faculty, friends and family members whose guidance, encouragement and support made this thesis possible.

Dave Dreese, I am grateful for the emphasis you placed on my personal learning and growth over the past two years. Your insightful feedback on my work and presentations, along with your effective leadership, has left a lasting impact.

Dr. Matthew Lear, who has been such a dependable and knowledgeable supervisor. Thank you for helping me define a manageable research scope. Your guidance and questions encouraged me to problem-solve, rather than simply providing answers.

Will Carsky, thank you for connecting me with this lab, being a daily encouragement in the office and for eagerly answering my questions. Your tips and tricks with Abaqus, along with the Python code framework you provided, were crucial to this thesis.

Denise Widdowson, your enthusiasm for research and learning is contagious. I am so grateful for the time you spent helping me diagnose models and code, and for dedicating hours to reviewing my thesis drafts in your free time so that I can be proud of this finished work.

Dr. Jean-Michel Mongeau for his helpful advice and responses to my questions throughout the entire process of finding a research group to thesis formatting.

My roommates, for supporting me with encouragement and “family meals” during the hectic times and for reminding me that, while this thesis is important, it doesn’t define me.

Finally, my deepest thanks to my parents and sisters, whose unconditional love, prayers, and encourage came through school visits, phone calls, texts and even a letter!

# Chapter 1

# Introduction

## Overview of Thick Composites in Bending

Thick fiber reinforced polymer (FRP) laminates have gained traction as load-bearing structures across multiple industries due to their exceptional mechanical properties, particularly their high strength-to-weight ratio [1]. An FRP is composed of multiple plies stacked together – this stacking is referred to as a layup. Each ply contains numerous fibers (illustrated by the red dots and lines in Figure 1) that are held in alignment by a polymer (epoxy), which serves as the binding or matrix material (indicated by the white boxes in Figure 1) [2], [3].

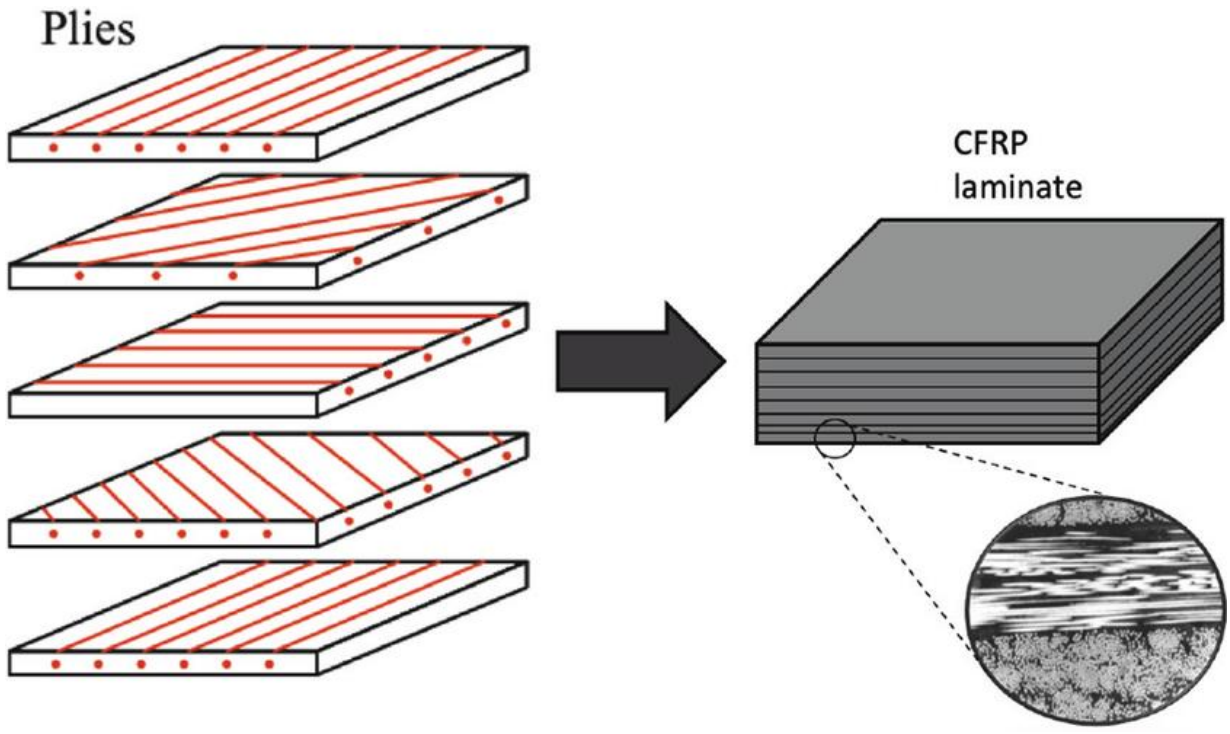


Figure 1. Internal structure of a multilayered FRP. The red lines depict the fibers, and the red dots indicate the fiber ends. Reprinted with permission from [3].

Over time, the epoxy cures and hardens around the fibers, bonding the layers together. This curing process is often accelerated using heat and pressure, typically by placing the composite in an oven or autoclave (a pressurized oven), which not only speeds up the process but can also enhance the material properties by improving fiber alignment and reducing voids [4]. Once cured, the resulting structure is referred to as a composite, as it consists of distinct but integrated components: the reinforcing fibers and the matrix material [5]. For the purposes of this thesis, thick composites are defined as having thickness $\geq$ 15mm (0.59 in). The fiber material in a composite can vary, but carbon fibers (CFRPs) and glass fibers (GFRPs) are the most common and are the only FRPs that are discussed in this thesis [6].

FRPs with fibers arranged at various angles (as shown in Figure 1) are typically classified as transversely isotropic materials. They exhibit different mechanical behavior in the fiber direction (in-plane) compared to the direction perpendicular to the fibers (through-thickness) [2]. In tension, FRP plies are strongest, but weaker under compression [7]. As indicated by the varying orientations of the red lines (fibers) in Figure 1, plies are often oriented in multiple directions to average their directional properties. Typically, no fibers cross between ply layers; meaning, the inter-laminar strength—the strength that holds the plies together—relies solely on the strength of the epoxy matrix and the adhesion strength of the fibers to the matrix. This characteristic makes the direction normal to the plies the weakest direction within an FRP laminate. As illustrated in Figure 2, when subjected to tension in the through-thickness direction, delamination (the separation of plies) is the most probable failure mode [2].

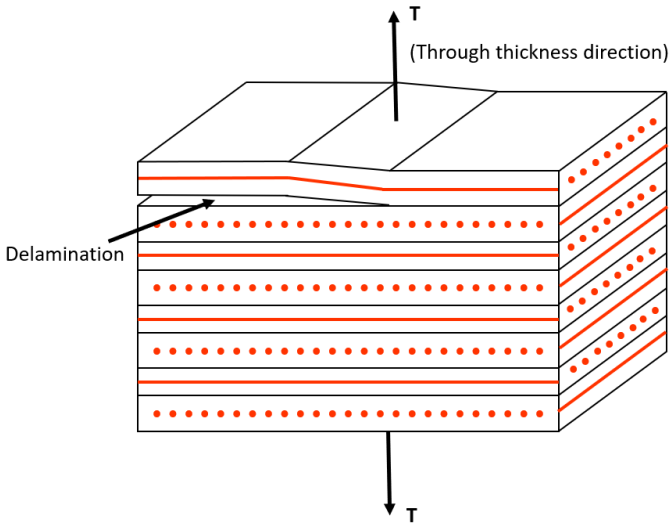


Figure 2. Diagram of delamination in a tensile specimen because of interlaminar adhesion strength.

To ensure that thick FRPs possess adequate strength for applications under multiaxial loading, experimental testing is a common verification method [8]. However, experimental tests can be time consuming and costly. As finite element (FE) modeling technology has advanced, researchers and industries have increasingly employed FE modeling to assist in the design of composite structures and joints relying on basic static tests to inform their FE models rather than creating exact experimental studies. Müzel et al. (2020) published a comprehensive review detailing the use of FE modeling for composite materials [9]. The authors discuss two primary approaches for modeling composites: micromechanics and macromechanics.

The micromechanics approach models the interactions between the composite fibers and the polymer matrix distinctly for each layer. Although this approach is significantly more computationally expensive and complex, it captures more of the irregular behavior of composites, such as delamination, and can account for manufacturing defects [10]. However, for large-scale applications, the micromechanics approach is typically employed to analyze the global response of composite structures. This method assumes smeared material properties (an

average of the fibers and matrix) for each directional aspect of the composite [11]. This thesis will utilize a macromechanics FE modeling approach to investigate the global response of thick composite joints, aligning with methodologies adopted in similar studies [12], [13], [14].

Bending loads will be applied to the joint, resulting in both tensile and compressive forces, which enhances the applicability of the results to future studies involving tension or compression. Figure 3 illustrates that under bending loads, tension is experienced by the plies on one face of the laminate (shown in orange), while compression is experienced by the plies on the opposite face (shown in blue).

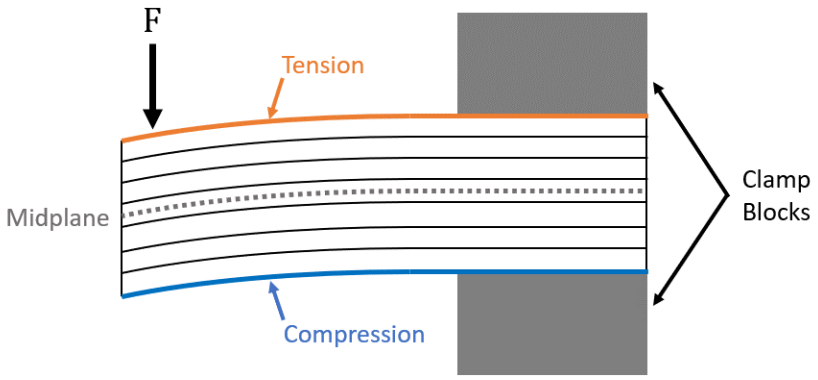


Figure 3. Diagram of an FRP under bending, showing tension in the fibers on one face of the laminate and compression in the fibers on the opposite face. Tension and compression forces are equal at the midplane.

As the thickness of a laminate increases, so does the risk of delamination and the likelihood of manufacturing defects, both of which can weaken the structure [15]. However, the larger geometry improves stiffness and strength, allowing thick composite joints to support higher loads than thinner ones without being as heavy as traditional high-strength materials [16]. This advantage has prompted multiple industries—including automotive, marine, defense, aerospace, and construction—to adopt thick FRPs for load-bearing applications, enabling the creation of robust and lightweight composite structures [1], [17]. Given their intended long service life, it is crucial to consider the durability and performance of these joints over time.

## Fatigue Life

Fatigue life was first documented in 1841 by Jean-Victor Poncelet, who noted that: "any spring subjected to a push-pull force will break under a load which is far smaller than the static breaking load" [18]. For many materials, the relationship between stress (S) and the number of cycles (N) before failure has been characterized and plotted on S-N Diagrams. While the fundamental principles of fatigue have evolved, this thesis focuses on high cycle fatigue (HCF). HCF occurs when a material is subjected to stress amplitudes below its yield stress, $\sigma_y$ at high frequencies until failure, which is typically after $10^6$ cycles, as shown in Figure 4 [19].

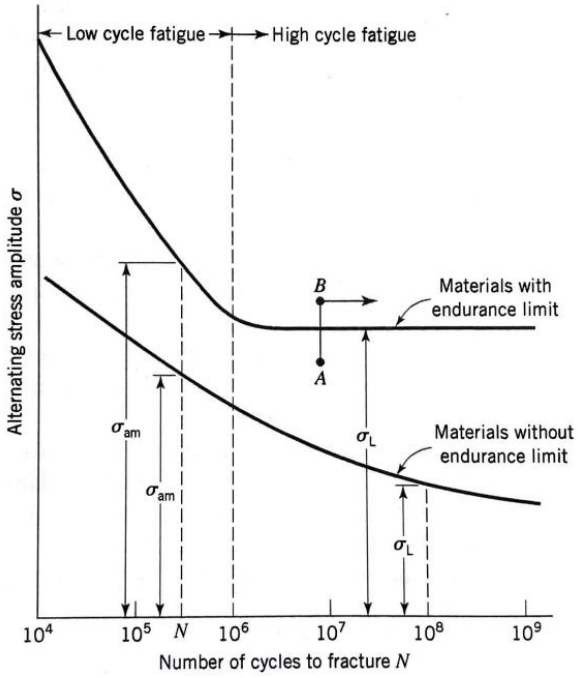


Figure 4. S-N curve showing the (alternating) stress amplitude vs number of cycles to failure for materials with and without endurance limits. Reprinted with permission from [19].

In 1867, Wöhler discovered that railway axle steel had an endurance limit $(\sigma_e)$ – a stress threshold below which the material could cycle indefinitely below without failure [20]. However, later studies revealed that this only applies to mild steels and some other steels [19].

Unlike metals, composite materials exhibit distinct failure mechanisms, making traditional fatigue prediction methods inadequate [21]. This challenge is amplified by the increasing thickness of composites, as thicker laminates tend to behave more unpredictably due to variations in internal stress distributions, localized delaminations, and potential defects within the material [15]. As a result, much of the fatigue behavior in thick composites is derived empirically, particularly in industrial applications [8], [10], [22].

Fatigue in metals, on the other hand, is well-characterized and more predictable, with established relationships that account for both both mean stresses ($\sigma_m$) and alternating stresses ($\sigma_a$). Mean stress is the average stress level around which the cyclic loading oscillates, while alternating stress is the variation in stress amplitude during the load cycle. It is important to account for mean stress in the fatigue life estimations, as it has a significant effect on how a material accumulates fatigue damage over time [19], [7]. One common method to predict fatigue in brittle materials is the Goodman relation, Equation (1), which estimates the fatigue life safety factor (SF). The SF quantifies fatigue life of the metal structure by representing the distance from the Goodman line:

$$\frac{1}{SF} = \frac{\sigma_a}{\sigma_e} + \frac{\sigma_m}{\sigma_{uts}} \tag{1}$$

where $\sigma_a$ is the alternating stress, $\sigma_e$ is the endurance limit, $\sigma_m$ is the mean stress, and $\sigma_{uts}$ is the ultimate tensile stress. $\sigma_e$ and $\sigma_{uts}$ are material properties.

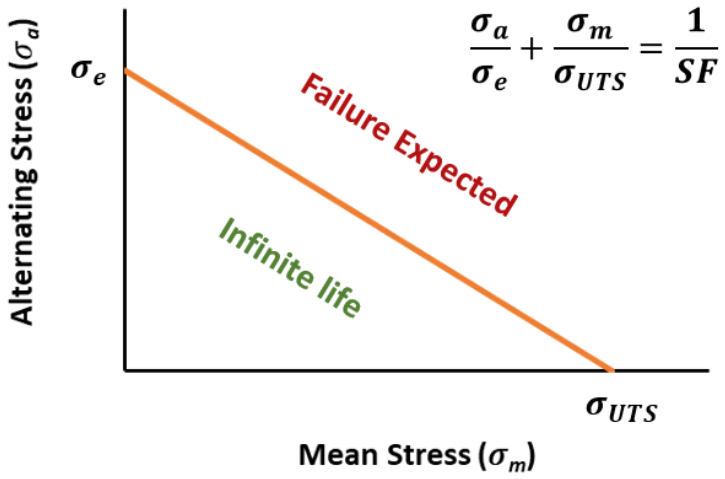


Figure 5. Graphical representation of the Goodman relation. Combinations of mean and alternating stress that lie below the line indicate infinite life, while stresses above it lead to failure.

The Goodman line (Figure 5) is typically plotted with $\sigma_m$ on the x-axis and $\sigma_a$ on the y-axis, as these stresses are often measured directly from experiments or FE models [7]. In HCF studies, if a point falls below the Goodman line, the material is expected to last indefinitely at that fatigue load. If a point lies above the line, failure is expected. To quantify the proximity to the line, the safety factor (SF) will be used. Although fatigue behavior in FRPs is typically determined experimentally, metal stress response can be reliably predicted using FE simulations, as it will be done in this study [8], [23], [24]. Running large FE models, however, requires considerable time and computing resources.

To reduce complexity and computational load, submodeling techniques can be employed, focusing on critical areas where failure is expected [25], [26], [27]. In submodeling, the full FE model is defined as the global model, and a smaller, more refined region is analyzed as the submodel. The submodel is linked to the global model through boundary conditions, which define the driving and driven interaction between the two as shown in Figure 6.

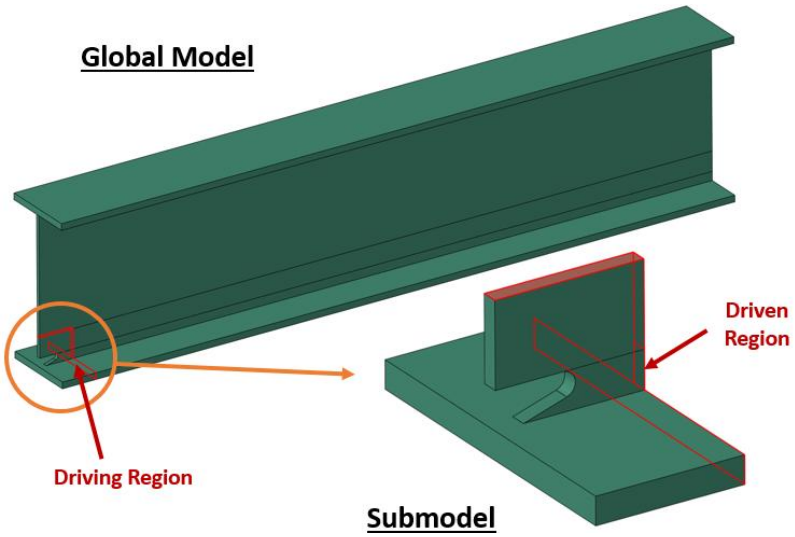


Figure 6. Diagram illustrating the “driving” and “driven” regions in submodeling.

Submodeling is efficient because, after an initial run of the global model, the submodel can be quickly altered and executed many times. Once the optimal geometry is determined through submodeling testing, this geometry is re-evaluated in the global model to confirm continuity. The size of the submodel needs to be determined carefully. If the geometry of the submodel is changed so that it affects the displacements on the boundary between the global model and submodel, the assumption that the boundary is the same as the global model is no longer true and the results of the submodel are invalidated [26].

In HCF studies, the submodeling process typically involves multiple steps, where nodal displacements from the global model are applied to the submodel at different stress levels [28]. This technique allows for a reduction in model size and complexity without sacrificing accuracy. Submodeling has been successfully applied to estimate and optimize fatigue life of structures by refining critical regions. Liu et al. estimated the fatigue life of an aging bridge by submodeling around the critical holes rather than simulating the entire bridge [27]. Predicting fatigue life is vital in designing components that will endure the stresses experienced over time. Submodeling

enables designers to focus on specific areas where failure is more likely – this is often around the bolts or joints [26], [27].

## Bolting in FRPs

Large structures across industries such as automotive, marine, defense, aerospace, and construction are increasingly being built using thick, load bearing composites [1], [17]. These structures are typically assembled by connecting individual parts via mechanical or adhesive joints [29]. There are multiple promising methods of joining FRPs such as adhesives [30], [31], [32], rivets [30], bolts, clinching, welding and others [33], [34]. This thesis will focus on bolted joints as they are the most common method [30]. Bolting is particularly advantageous in large assemblies as it allows for disassembly and repair. However, a downside to bolting is that it requires drilling holes into the composites, breaking fibers and weakening the area around the holes and creating a stress concentration [35]. When subjected to bending loads, the contact between the bolt shaft and the composite further exacerbates these stress concentrations, reducing the fatigue life of the joint [31].

To maximize the fatigue life of a bolted joint, it is important to understand the mechanical response and failure modes [36], [37]. Figure 7 illustrates the three most typical failure mechanisms for bolted FRP joints under tensile loading [30].

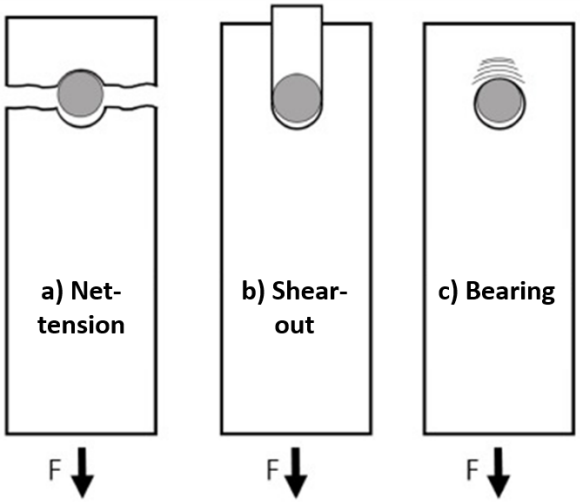


Figure 7. The typical failure modes for bolted composite under tension. a) net-tension failure, (b) shear-out failure, (c) bearing failure. Modified with permission from [38].

Net-tension failure (Figure 7a) occurs when the area around the hole exceeds its ultimate tensile strength, leading to fracture. Shear-out failure (Figure 7b) occurs when the distance between the hole and the edge of the material is unable to support the shear forces generated by the load. Bearing failure (Figure 7c) occurs when the bolt crushes the material near the hole. Bearing failure is gradual, leading to material degradation and deformation of the hole over time. Bearing failure is expected to be the primary failure mode in these experiments due to bolt preload, which helps mitigate more catastrophic failures like net-tension and shear-out [39]. Bolt preload (visually shown in Figure 8) refers to the compressive force applied to the bolt by tightening the nut prior to loading the structure, typically specified by torque [40].

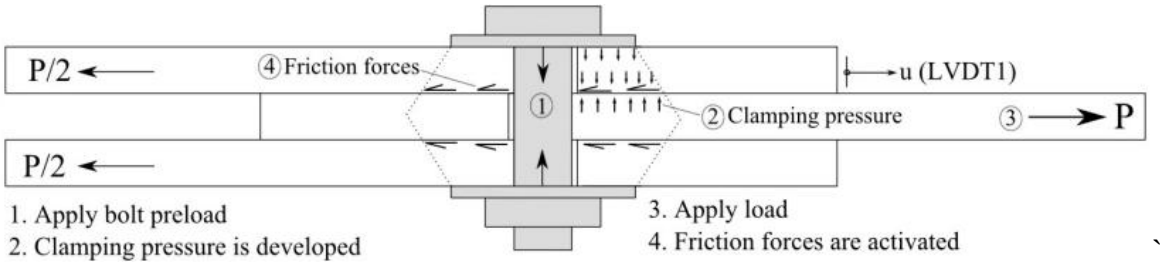


Figure 8. Preloaded bolted joint and resulting forces. Reprinted with permission from [40].

Improperly designed joints can become points of damage initiation, leading to ultimate failure of the entire structure [39]. Wang et al. demonstrated that catastrophic bearing damage can occur without sufficient lateral support (perpendicular to the load) [41]. Lateral support also increases joint stiffness and reduces contact openings within the joint. Repeated contact openings, particularly under high cycle fatigue, significantly decrease fatigue life [42]. Numerous studies have shown that lateral support can be enhanced by increasing bolt preload [43], [44], [45] and bolt interference [31], [43], [46], [47], [48]. Preloading the bolt creates a clamping force between the bolt head and the composite, which increases lateral support by increasing friction that prevents the bolt from shifting sideways [43]. Washers can further improve clamping area and lateral support, reducing the risk of joint failure [44].

Increasing bolt interference decreases local stress concentrations and adds lateral support to the joint by inducing radial forces perpendicular to the load [31], [46]. Bolt interference is defined as a dimensional difference in Equation (2):

$$\text{Interference} = \emptyset_{bolt} - \emptyset_{hole} \tag{2}$$

where $\emptyset_{bolt}$ is the diameter of the bolt and $\emptyset_{hole}$ is the diameter of the bolt hole. Interference can also be measured as a percentage as in Equation (3):

$$\text{Interference \%} = \frac{\emptyset_{bolt} - \emptyset_{hole}}{\emptyset_{hole}} * 100\% \tag{3}$$

Figure 9 illustrates the three types of classifications of bolt fits: interference fit (Figure 9a), neat fit (Figure 9b), and clearance fit (Figure 9c).

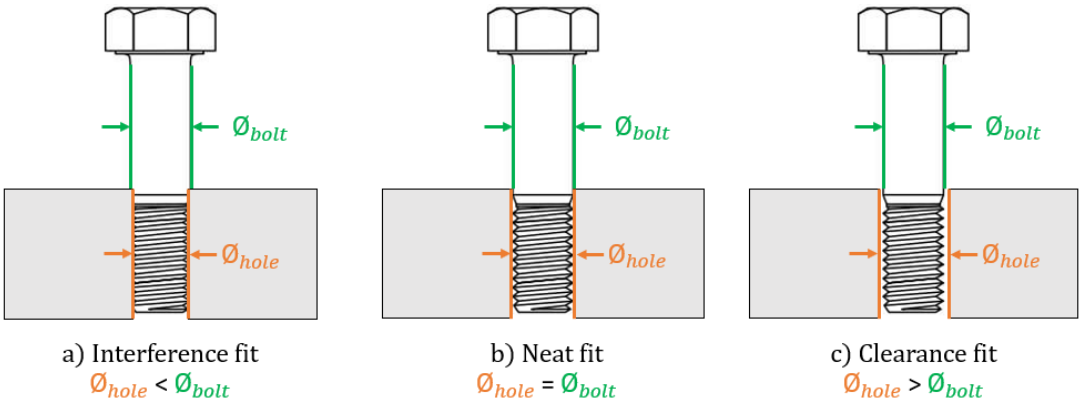


Figure 9. Diagram defining the three types of bolt fits: a) interference fit ($Ø_{hole} < Ø_{bolt}$), b) neat fit ($Ø_{hole} = Ø_{bolt}$), and c) clearance fit ($Ø_{hole} > Ø_{bolt}$).

Interference fit bolts have been shown to improve both joint strength and fatigue life [49], [50]. Raju et al. concluded that a 0.5-2% interference fit bolt increased load sharing by 10% compared to neat fit or clearance fit bolts [31]. Additionally, interference fit bolts reduce alternating stress amplitude, a critical factor in fatigue life prediction using the Goodman relation, as shown in Figure 10. Different studies have found varying optimal interference fit percentages. For instance, Cao et al. reported that 0.5% interference minimized damage [46], while Wei et al. concluded that 1.8% or 3% interference was optimal, depending on the type of load [48].

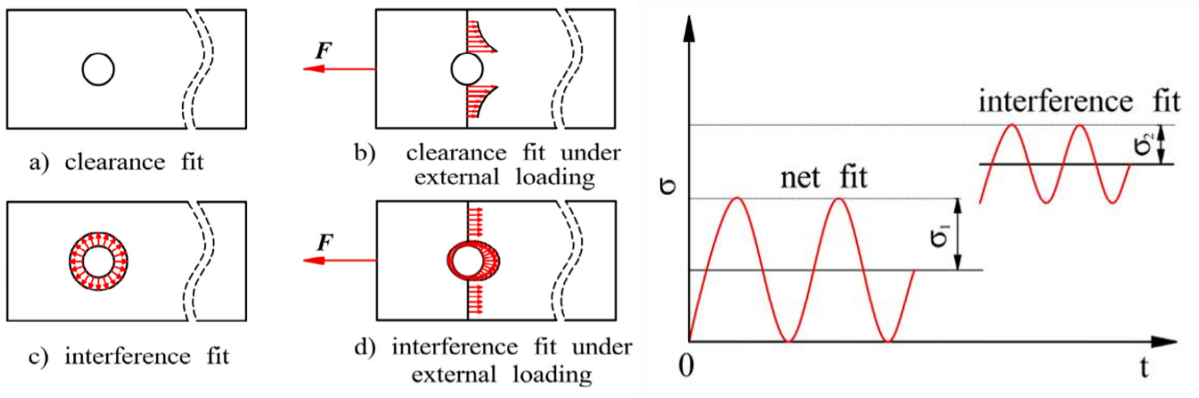


Figure 10. Images a-d show force distributions for clearance fit and interference fit bolts. The graph highlights that neat fit bolts exhibit lower $\sigma_m$ but larger alternating stress ($\sigma_1$), whereas interference-fit bolts show higher $\sigma_m$ but smaller alternating stress ($\sigma_2$). Reprinted with permission from [46].

While interference fit bolts are common in metallic joints, they are challenging to implement in FRPs due to the material's low inter-laminar strength. When oversized bolts are inserted, the plies on the exit face of the FRP tend to delaminate [51], making interference fit bolts less suitable for composite joints [52]. To address this issue, researchers have developed alternative fastening methods that preserve the benefits of interference fits without causing the same installation damage.

## Bolt Sleeves

One potential solution for overcoming the challenges of interference fit bolts in composites is the use of bolt sleeves. In 1982, Cole et al. explored several fastener systems designed to create interference fits in composite materials without causing installation damage and recommended further research into bolt sleeves [53]. Figure 11 illustrates a method that uses deformable sleeves, which have been the subject of recent studies by Xu et al. for their potential in improving fatigue life [52], [54], [55].

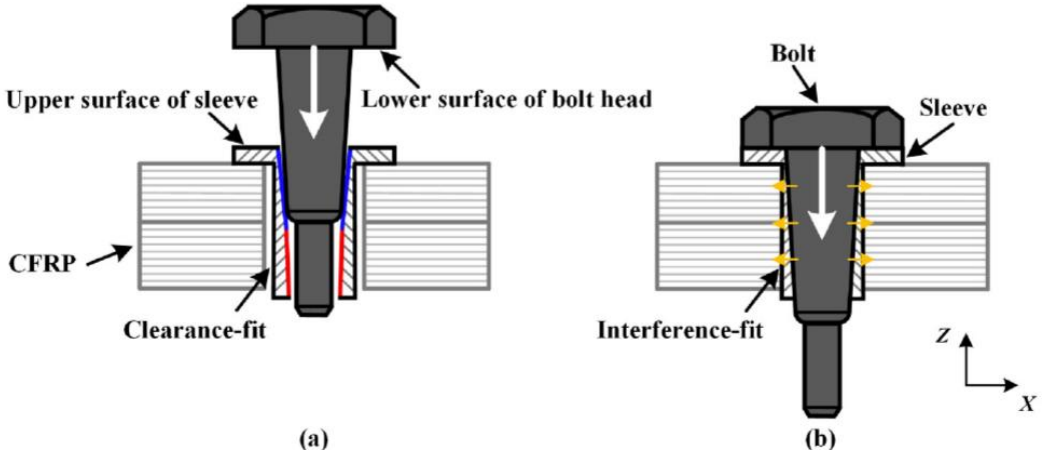


Figure 11. Installation diagram for a ductile sleeve creating a bolted joint with an interference fit. Reprinted with permission from [54].

These ductile sleeves are initially clearance fit into the FRP hole. As the tapered bolt is inserted, the sleeve plastically deforms to create an interference fit with the hole. The force exerted on the FRP is radial (as indicated by the yellow arrows in Figure 11b), reducing the risk of delamination. One experiment reported a 33% increase in the initial failure load of the joint by adding bolt sleeves [55]. Another study on sleeve geometry found that increasing the sleeve's thickness reduced plastic deformation, resulting in more uniform radial displacement and less interference damage [52]. However, Xu et al.'s experiments have only involved thin composites (< 3.48 mm or < 0.137 in) and have not quantitatively measured fatigue life, leaving the fatigue behavior of bolt sleeves in thick FRPs largely unexplored.

Figure 12 shows typical metallic inserts, another type of bolt sleeve. These inserts are installed either with adhesive or by cold expansion [56], [57]. In cold expansion, the sleeve is cooled (shrunk) before insertion, then allowed to warm and expand, creating an interference fit.

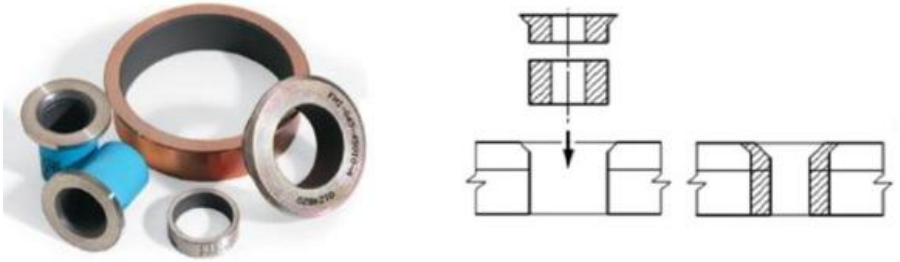

Figure 12. Metallic inserts and installation. Reprinted with permission from [56].

Metallic inserts enhance joint bearing strength and have been widely used to repair metallic joints by enlarging holes and inserting the inserts (Figure 12), instead of replacing the entire structure [56]. A similar approach is applied to CFRPs, though drilling holes in composites breaks fibers and weakens the area around the hole. To avoid this, metallic inserts can be embedded into the composite before curing, allowing the insert to become structurally integrated with the composite (Figure 13) [58].

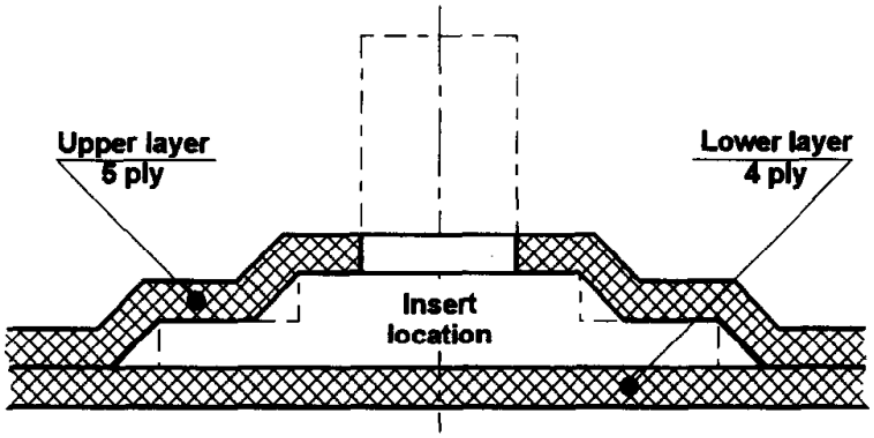


Figure 13. Composite laminate with embedded metallic insert. Reprinted with permission from [58].

For embedded inserts, fibers are directed around the metallic insert to preserve the composite's structural integrity by minimizing fiber breakage [59], [60]. However, there are some downsides. For example, embedded inserts can initiate delamination if they twist and pry apart the composite layers [61]. Metallic inserts also resist deformation under preload, unlike FRPs which experience creep and lose preload over time [40]. Maintaining bolt preload is critical for preventing contact openings in the joint and maximizing fatigue life. Additionally, other types of bolt sleeves are being developed for various purposes, such as improving joint strength and deformation capacity [62].

This thesis will introduce a type of bolt sleeve known as a "shear sleeve", designed to increase the joint's fatigue life. Unlike the deforming bolt sleeves and metallic inserts previously discussed, shear sleeves have two primary functions: to carry the shear loads experienced by the bolt and to be installed with interference to prevent contact openings in the joint. As shown in Figure 14, thick composites subject to bending loads develop larger shear forces ($\tau$) at the interfaces between the clamp blocks and the composite. This increase in shear force is due to the greater distance between the midplane and the edge of the composite, which creates a longer

lever arm than that in a thin composite. A longer lever arm amplifies the bending moment applied to the joint, resulting in higher lateral shear stresses that are transferred to the shear sleeve.

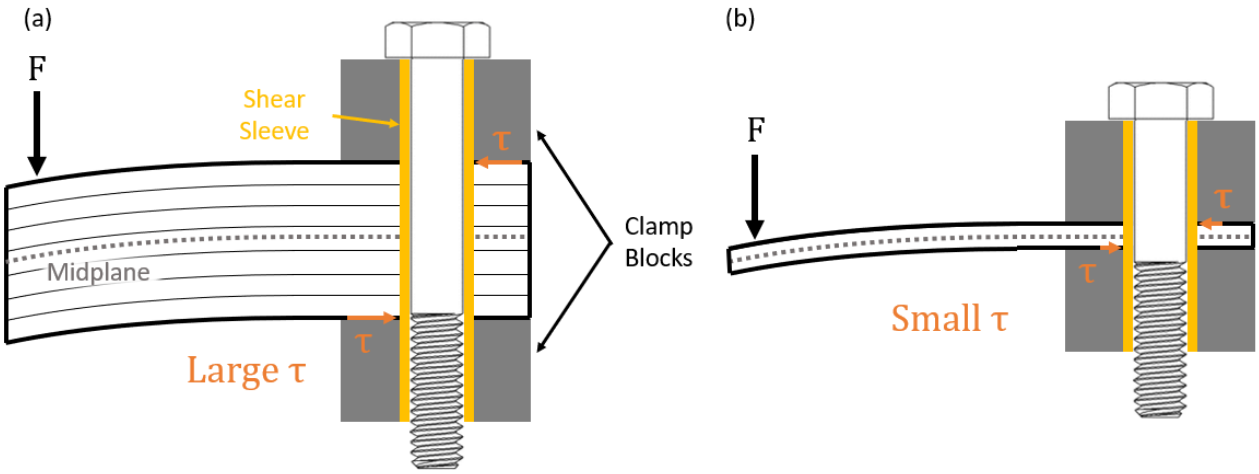


Figure 14. Diagram of a shear sleeve and bolt under a bending load (F). The orange arrows show the lateral shear stress ($\tau$) on the sleeve in bending. a) Thick FRPs experience higher shear forces ($\tau$) than b) thin FRPs due to the larger lever arm amplifying the bending moment.

For these shear sleeves, an interference fit will be created via the cold expansion method [57]. This interference helps the sleeve absorb alternating shear forces, reducing the fatigue stresses on the bolt itself. By ensuring a clearance fit between the bolt and the sleeve, the bolt primarily handles preload forces while the sleeve takes on the cyclic shear loads. This design prevents contact openings in the joint, enhancing its fatigue life. Both the level of interference during installation and the sleeve thickness are critical factors influencing the sleeve and joint's overall fatigue performance.

## Research Goal

The aim of this work is to quantify the effects that shear sleeve geometry have on the sleeve's fatigue life in a thick composite joint. Specifically, this work investigates how variations in shear sleeve interference (Figure 15a) and thickness (Figure 15b) influence fatigue performance of the sleeve, with the ultimate goal of providing design recommendations for improved fatigue life in composite bolted joints.

Objective 1: Establish a means to evaluate fatigue performance for a composite joint with a shear sleeve

Objective 2: Define the design space bounds and parametric sweep exploration thereof

Objective 3: Evaluate the effects of shear sleeve geometry to find and recommend optimal geometry

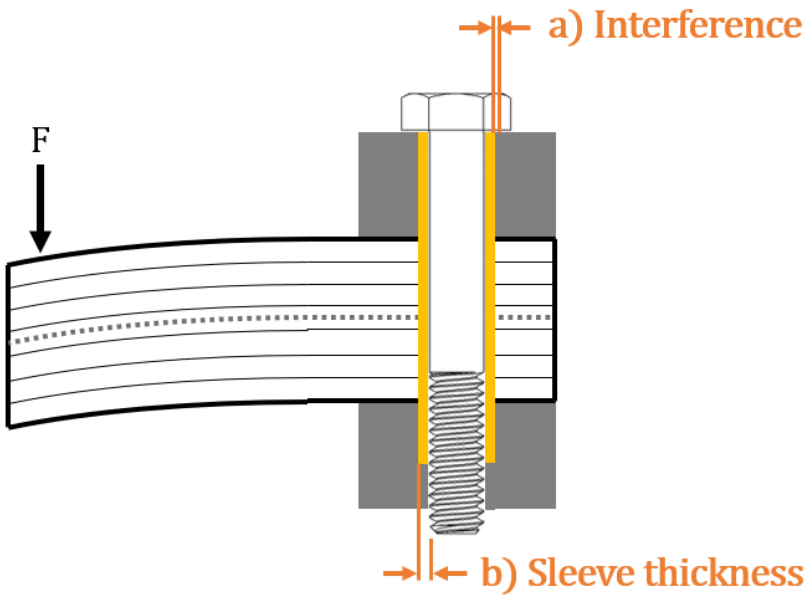


Figure 15. Diagram of parameters investigated in this study: a) shear sleeve interference and b) thickness.

Chapter 1 has provided background information on thick FRPs under bending loads, an overview on fatigue life, the effect of interference fits in bolted FRP joints, and descriptions of prior research done on bolt sleeves. Chapter 2 explains the methods and materials used in this thesis, including the development of the FE submodel and the method for calculating fatigue life of the shear sleeves. Chapter 3 then presents the results of the parametric sweep and discusses the results. A brief conclusion and shear sleeve design recommendations are provided in Chapter 4, and a series of appendices are attached for further details where necessary.

# Chapter 2

# Methods

## Modeling and Materials

The work presented in this thesis focuses on modifying the geometry of shear sleeves within an FE model of a complex bolted FRP joint subjected to a bending load. The FE model was developed and executed using Abaqus CAE 2023 [63]. To establish confidence in the modeling techniques, individual aspects of the FE model were created and validated separately, with lessons learned applied to the overall research presented here.

The first aspect addressed was accurately modeling interference fits and validating a model against closed-form solutions [64]. The detailed process of this step is provided in

Appendix A: Modeling interference fits, where the FE results were shown to correlate with governing equations within a 2% margin of error. The second focus was on simulating the behavior of thick, bolted composites under bending loads. This work is outlined in

Appendix B: Modeling thick, bolted CFRPs under bending loads, where the FE model was compared to experimental strain results from the literature showing strong agreement [12], [13].

Building on these foundational models, this thesis focuses on a more complex, multi-material bolted joint model, which includes the entire test frame fixture. However, since the primary focus of this study is on the submodel and shear sleeves, only the submodel will be discussed in detail [27]. Figure 16 highlights the key materials in the global model, the material geometries and locations, and the direction of the applied load.

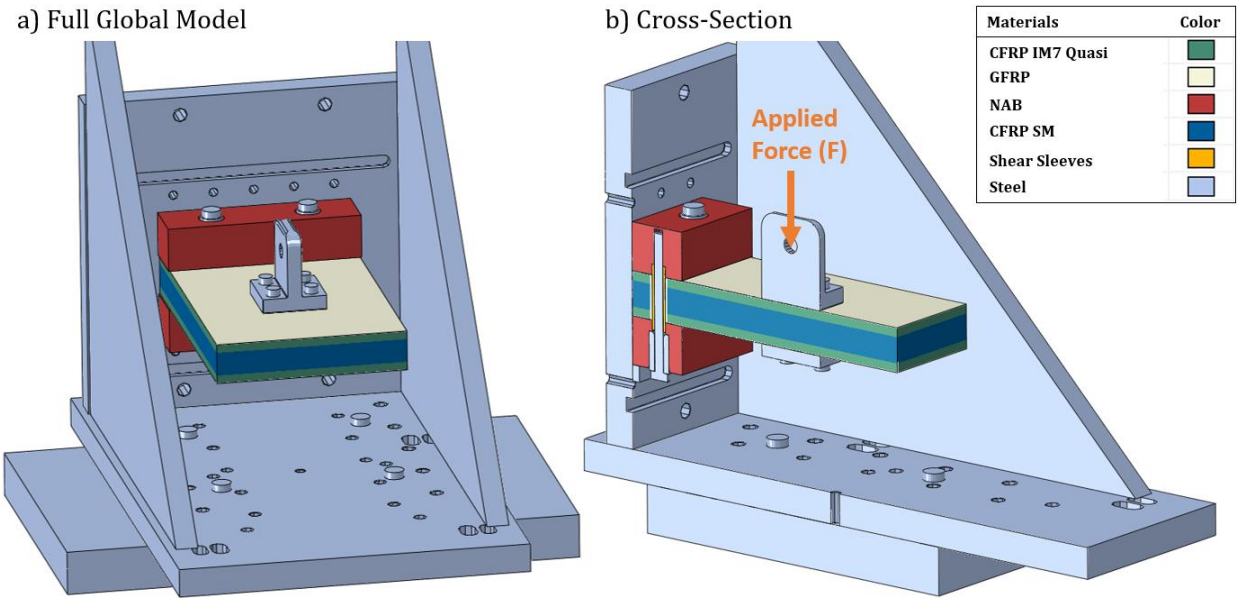


Figure 16. a) Full global model and b) cross-section view highlighting the different materials. It also indicates direction and location of the applied load (F).

Table 1 highlights each material's properties including the transversely isotropic nature of the composite materials by indicating both the in-plane (ip) and through-thickness (tt) material properties [7]. Within the global model, it is also assumed that no materials will reach yielding, therefore yield stresses ($\sigma_y$) are not included in Table 1 or Abaqus.

**Table 1. Material properties in global model: 'ip' for in-plane and 'tt' for through-thickness**

| Material | Young's Modulus ($E$) [ksi] | Poisson's Ratio | Shear Modulus [ksi] |
|---|---|---|---|
| CFRP IM7 Quasi | $E_{ip} = 8{,}405$<br>$E_{tt} = 1{,}500$ | $\nu_{ip} = 0.302$<br>$\nu_{tt} = 0.302$ | $G_{ip} = 3{,}227$<br>$G_{tt} = 900$ |
| GFRP | $E_{ip} = 2{,}687$<br>$E_{tt} = 1{,}395$ | $\nu_{ip} = 0.288$<br>$\nu_{tt} = 0.247$ | $G_{ip} = 1{,}043$<br>$G_{tt} = 500$ |
| CFRP SM | $E_{ip} = 5{,}600$<br>$E_{tt} = 1{,}500$ | $\nu_{ip} = 0.252$<br>$\nu_{tt} = 0.3$ | $G_{ip} = 1{,}980$<br>$G_{tt} = 700$ |
| NAB | $E = 17{,}000$ | $\nu = 0.34$ | - |
| Shear Sleeves | $E = 29{,}880$ | $\nu = 0.3$ | - |
| Steel | $E = 30{,}000$ | $\nu = 0.3$ | - |

The global model, which represents a complex joint, requires multiple loading steps to converge to a solution and capture historical effects, as outlined in Table 2. For each step, the time period was set to 1 and nonlinear geometric effects (Nlgeom) were included in the analysis to account for large deformations and to allow the bending load to be consistently applied perpendicular to the composite during loading.

**Table 2. Global model loading steps and descriptions**

| Step Number | Step Name | Description |
|---|---|---|
| 1 | Initiate Contact | Required first step in Abaqus [63] |
| 2 | Interference fit | Increase outer diameter of the shear sleeve to create the interference fit |
| 3 | Preload Fixture Bolts | Preload fixture bolts that hold the frame together and to the test bed |
| 4 | Preload Pin Bolts | Preload the three vertical pin bolts that run through the shear sleeves and compress the composite |
| 5 | Preload Hold Down Bolts | Preload the bolts attaching the clamp blocks to the back fixture plate |
| 6 | Compression (3.33 kip) | Apply a 3.33 kip downwards compressive force (F) on the composite beam (see Figure 16) |
| 7 | Compression (5 kip) | Increase the compressive force to 5 kip |
| 8 | Compression (10 kip) | Increase the compressive force to 10 kip |
| 9 | Compression (25 kip) | Increase the compressive force to 25 kip |
| 10 | Compression (50 kip) | Increase the compressive force to 50 kip |

The incremental compression steps allow for the study of fatigue life changes under varying loads. HCF will occur between two of these compression steps, resulting in a low stress state ($\sigma_{low}$) and a high stress state ($\sigma_{high}$) used to calculate alternating and mean stress, which are inputs for the Goodman relation, Equation (1). The endurance limit ($\sigma_e$) and ultimate tensile stress ($\sigma_{uts}$) are material properties for this calculation. The shear sleeves are made of 52100

steel, with $\sigma_{uts} = 292$ ksi and yield stress ($\sigma_y$) $= 279$ ksi [7]. Although $\sigma_e$ is not explicitly documented for 52100 steel, it can be estimated from $\sigma_y$ and $\sigma_{uts}$ using Figure 17. This estimation yields a ductility parameter of approximately 0.045. From Figure 17, the ratio of endurance limit to the yield stress is 0.43, resulting in $\sigma_e \approx 120$ ksi. These values for $\sigma_e$ and $\sigma_{uts}$ will be used to estimate fatigue life using the Goodman relation.

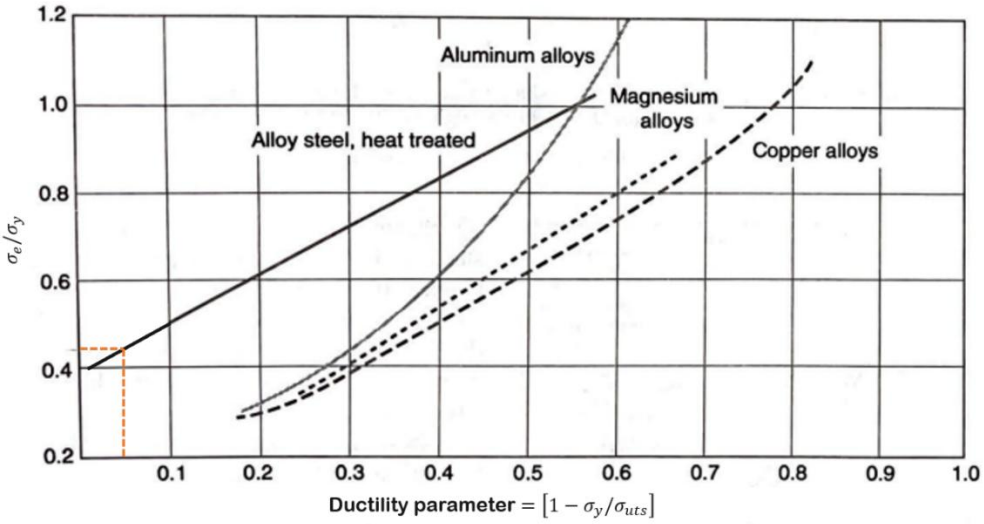


Figure 17. Plot for estimating fatigue endurance limits ($\sigma_e$) for common structural alloy groups, with 52100 steel estimates overlaid. Modified with permission from [7].

Based on prior experimental testing of the global model, FE results for strain closely match experimental strain gage data, with a margin of error of 5%. This provides confidence that both global model stresses and strains, as well as those in the submodel will align with physical experimental studies.

## Submodeling Approach

As presented in Chapter 1, Fatigue Life section, submodeling can be an effective method for reducing computational demand without sacrificing accuracy, particularly when focusing on

a small region of interest [25], [26], [27]. This approach is utilized in the current study to model the region around the shear sleeves in the bolted joint. To build confidence in the submodeling technique, a preliminary experiment was conducted, as described in Appendix C: Submodeling and parametric sweeps.

To focus on the response of a single shear sleeve, the submodel region can be significantly smaller than the global model, as highlighted by the purple section in Figure 18 and is shown in closer detail in Figure 19.

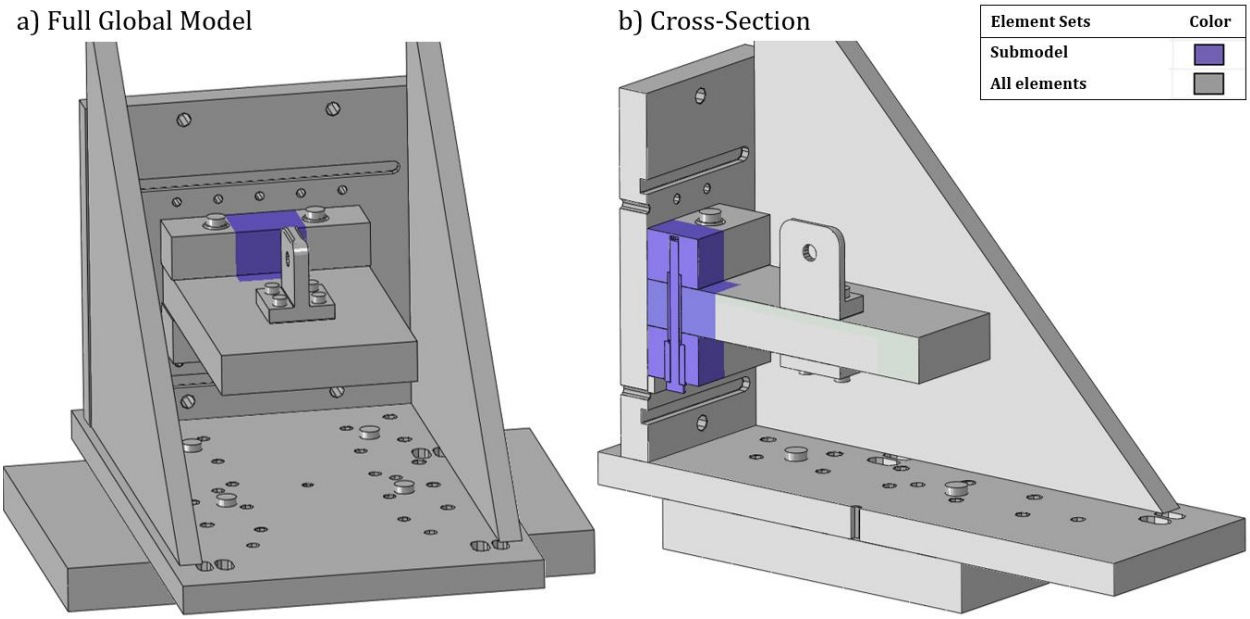


Figure 18. Submodel region highlighted in purple within the a) full global model and b) cross-section view.

The submodel (Figure 19) captures the complex joint comprised of six different materials. Three of these materials make up the composite: a standard modulus (SM) CFRP, a quasi-isotropic intermediate modulus (IM) CFRP, and a GFRP skin that encases the entire composite, including a GFRP bushing around the shear sleeve. The remaining materials include

the bolt, made of general steel, the shear sleeve, composed of 52100 steel, and the clamping blocks, made from a nickel-aluminum-bronze (NAB) alloy.

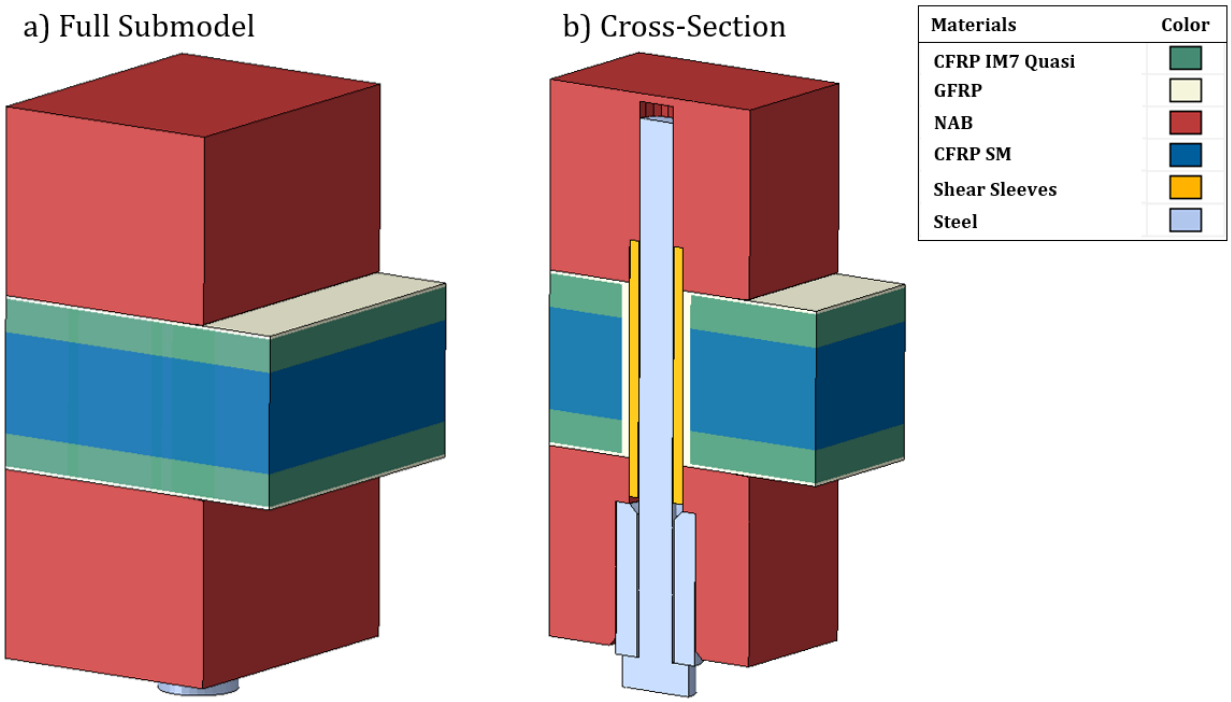


Figure 19. Diagram of submodel region highlighting the different materials and their locations.

In this study, boundary conditions (BCs) were applied between the driving region of the global model and the driven region of the submodel, constraining degrees of freedom (DOFs) 1, 2, and 3. The submodel's BCs at the interface to the global model were updated at each global step to account for displacement changes as the load increased. Since the global model results define the BCs at each step for the submodel, geometric variations in the submodel can be tested without rerunning the global model every time.

For the shear sleeve interfaces, surface-to-surface contact was specified using an interference fit option, where secondary node overclosure was gradually removed during each loading step to avoid excessive surface penetration. Interactions between the bolts, clamp blocks and the test fixture were managed using tie constraints, while general contacts with a friction

coefficient of ($\mu = 0.14$), determined by prior experimental studies, were applied for the remaining contacts. With the reduced size and a more refined mesh, the submodel was meshed with 44,818 linear hexahedral elements of type C3D8I compared to the global model which was meshed with 419,049 linear hexahedral elements of type C3D8I and quadratic tetrahedral elements of type C3D10.

## Parametric Study

Using the developed submodel, a parametric study will be conducted to investigate the effects of interference fit and sleeve thickness on the fatigue life of the shear sleeve. This will be conducted using a similar methodology to Shaheen et al, where the effects of each parameter on fatigue life will be studied using an FE submodel [62]. Fatigue life will be quantified by the fatigue life safety factor (SF) as previously defined in the Goodman relation, Equation (1). Similar studies have employed FE modeling to analyze how changes in geometry affect other parameters, such as stiffness or shear strength [65], [28], [66]. Appendix C: Submodeling and parametric sweeps provides a reference for the development of a simpler Python code to conduct a parametric sweep, which served as a foundation for the code detailed in Appendix D: Parametric sweeps Python code.

To set up the parametric study, ranges for interference and thickness must first be defined. Submodel results become invalid if the FE model fails to converge or if stress on the driven region are significantly affected. Based on preliminary experimentation, the minimum interference and thickness that allowed the model to converge were 0 in for interference and 0.05 in for thickness, as shown in Figure 20a. The maximum interference was approximately 0.01 in,

and the maximum thickness was approximately 0.20 in before significant changes in the edge stresses occurred as seen in Figure 20b.

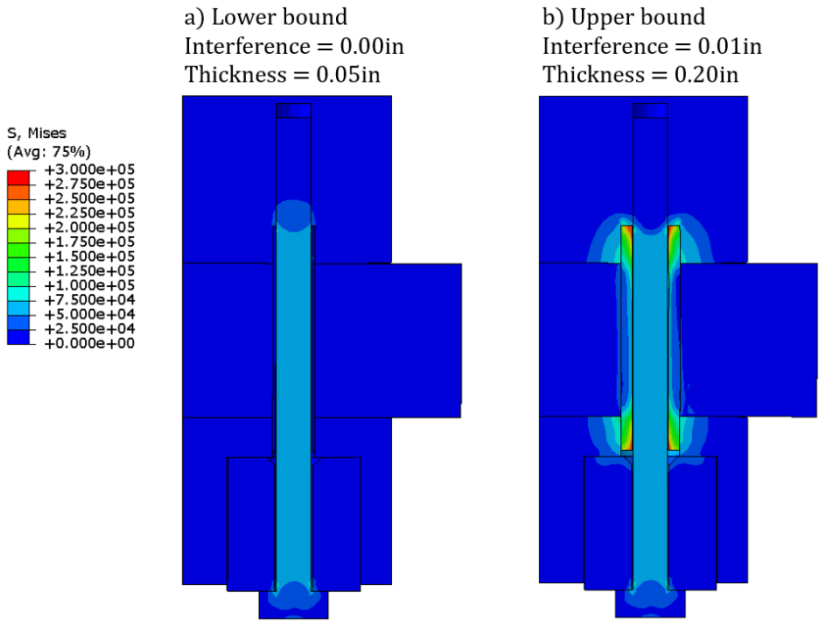


Figure 20. Preliminary experimentation to determine ranges of interference and thickness parameters found that the a) lower bound to be 0 in interference and 0.05 in thickness and b) upper bound to be 0.01 in interference and 0.20 in thickness.

The step size between iterations was selected to ensure a sufficiently dense grid for generating an accurate surface plot. The number of steps for interference was set higher than for thickness to capture finer variations in that parameter. Based on preliminary experimentation, the parameter ranges and step sizes for the parametric sweep are summarized in Table 3.

**Table 3. Parametric sweep ranges and step sizes for shear sleeve interference and thickness**

| Parameter | Minimum [in] | Maximum [in] | Step Size [in] | Number of Steps |
|---|---|---|---|---|
| Interference | 0 | 0.01 | 0.0005 | 21 |
| Thickness | 0.05 | 0.20 | 0.01 | 16 |

With the ranges and step sizes determined, two nested for loops will iterate through each combination of interference and sleeve thickness for a total of 336 iterations. For each case, the geometry in Abaqus will be edited, the submodel will be resolved, and the results of each job will be stored in a text file. The full code developed for this process can be found in Appendix D: Parametric sweeps Python code.

To determine the effects of interference and thickness on fatigue life (SF), post-processing is required. The function "getFatigueLife" iterates through each element in the shear sleeves at a specified low-stress step ($\sigma_{low}$) and high-stress step ($\sigma_{high}$) (the two compressive loads that fatigue is occurring between) and calculates a SF for each element in the shear sleeve using the Goodman relation. Alternating stress ($\sigma_a$) and mean stress ($\sigma_m$) are required by the Goodman relation. Equation (4) shows how $\sigma_a$ is calculated:

$$\sigma_a = \frac{\sigma_{high} - \sigma_{low}}{2} \tag{4}$$

Equation (5) shows how $\sigma_m$ is calculated:

$$\sigma_m = \frac{\sigma_{high} + \sigma_{low}}{2} \tag{5}$$

Next, $\sigma_a$, $\sigma_m$, $\sigma_e$, and $\sigma_{uts}$ are input into the Goodman relation to calculate a SF for each element. The lowest SF within the sleeve will be taken as the SF for that particular geometry. Although high localized stresses in a single element may result in an artificially low or overly conservative SF in some cases, this method ensures that the critical behavior of the sleeve is captured. This process is repeated for each combination of interference and sleeve thickness. The results are then plotted using Matlab to evaluate how each parameter affects $\sigma_a$, $\sigma_m$ and SF.

# Chapter 3

# Results and Discussion

## Submodel versus Global Model Correlation

To ensure that the submodel accurately reflects the global model, both qualitative and quantitative comparisons were made. Stress and displacement contour plots for the entire submodel and the shear sleeves were examined for visual agreement and percentage differences between the peak values of stress and displacement were calculated to quantify the correlation. The percentage difference between the submodel and global model values was determined using:

$$\% \text{ Difference} = \frac{|V_{submodel} - V_{global}|}{|V_{global}|} * 100\% \quad (6)$$

where $V_{submodel}$ and $V_{global}$ represent the values for each model's stress and displacement.

Stress (Figure 21a) and displacement (Figure 21b) contour plots show strong visual correlation in stress and displacement patterns between the submodel and global model.

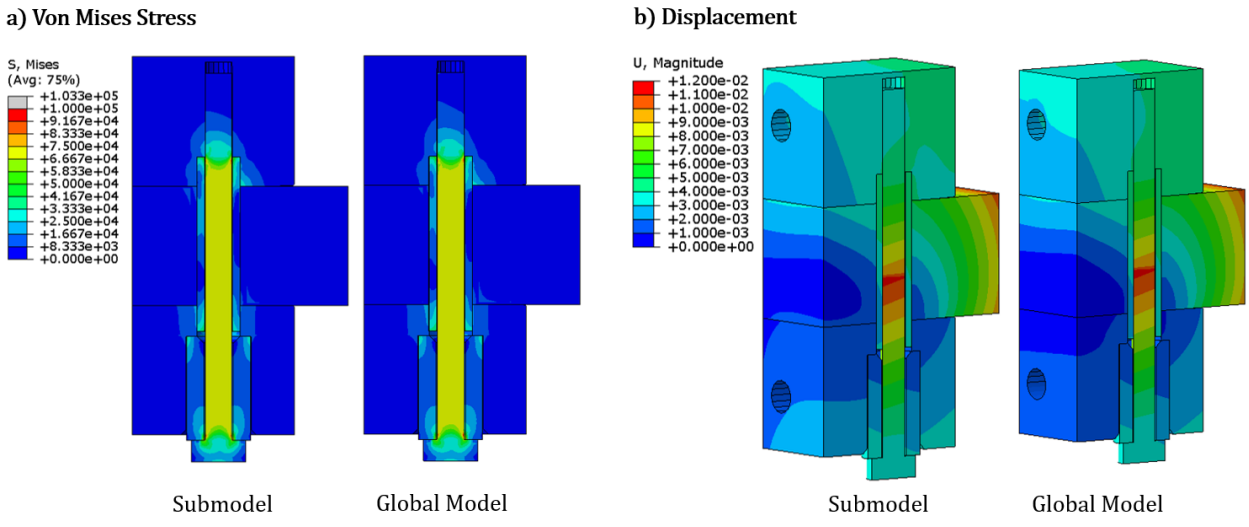


Figure 21. Diagram of submodel and global model with a) Von Mises stress and b) displacement contour plots to show qualitative agreement.

Figure 22 focuses on the stress and displacement contour plots within the shear sleeves, showing minor discrepancies but an overall strong qualitive correlation.

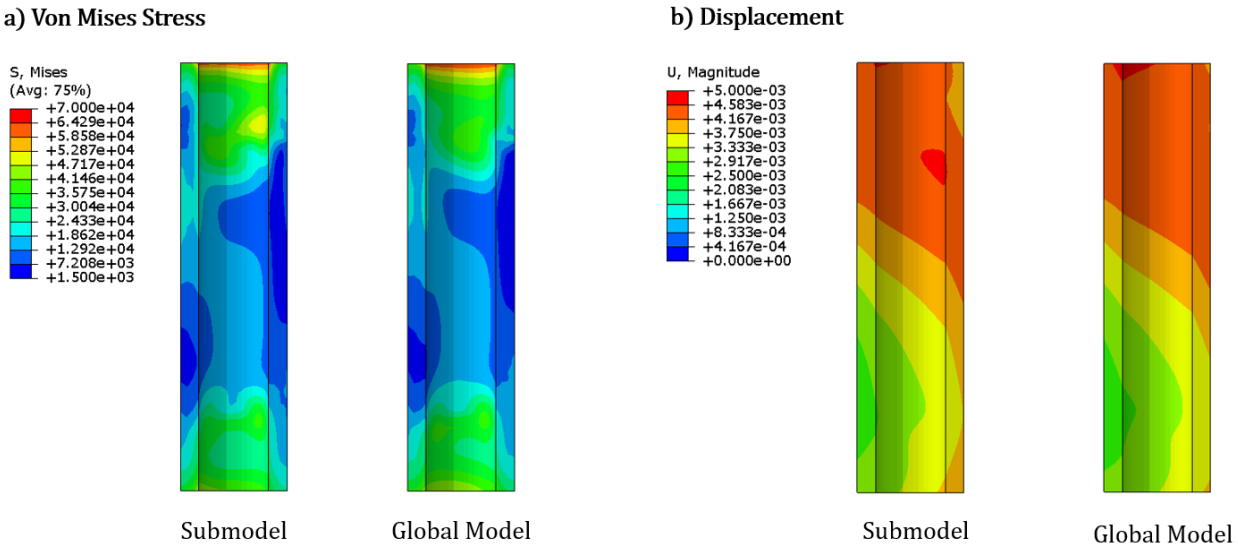


Figure 22. Diagram of shear sleeves within the submodel and global model with a) Von Mises stress and b) displacement contour plots to show qualitative agreement.

To quantitatively compare the submodel and global model, a percentage difference was calculated based on the maximum value in the FE model for both stress and displacement in the entire submodel region and single shear sleeve. These calculations, summarized in Table 4, reveal that no percentage difference exceeds 3.5%. This quantitative analysis confirms a high degree of confidence in the submodel's ability to replicate the global model's behavior.

**Table 4. Quantitative comparison of stress and displacements peaks in submodel and global model.**

| | Parameter | Submodel max | Global model max | Percentage Difference |
|---|---|---|---|---|
| Submodel Region | Von Mises Stress [ksi] | 103.3 | 103.3 | 0.00% |
| | Displacement [in] | 0.01146 | 0.01146 | 0.00% |
| Shear Sleeve | Von Mises Stress [ksi] | 68.79 | 69.97 | 1.69% |
| | Displacement [in] | 0.00466 | 0.00482 | 3.26% |

## Parametric Study Results (3.33 – 10 kip)

With the correlation between the submodel and global model established, the parametric study was conducted using the FE submodel to sweep over the range of interferences and thicknesses as previously defined in Table 3. The effects of each of these variables on alternating stress (Figure 23a) and mean stress (Figure 23b) was first investigated.

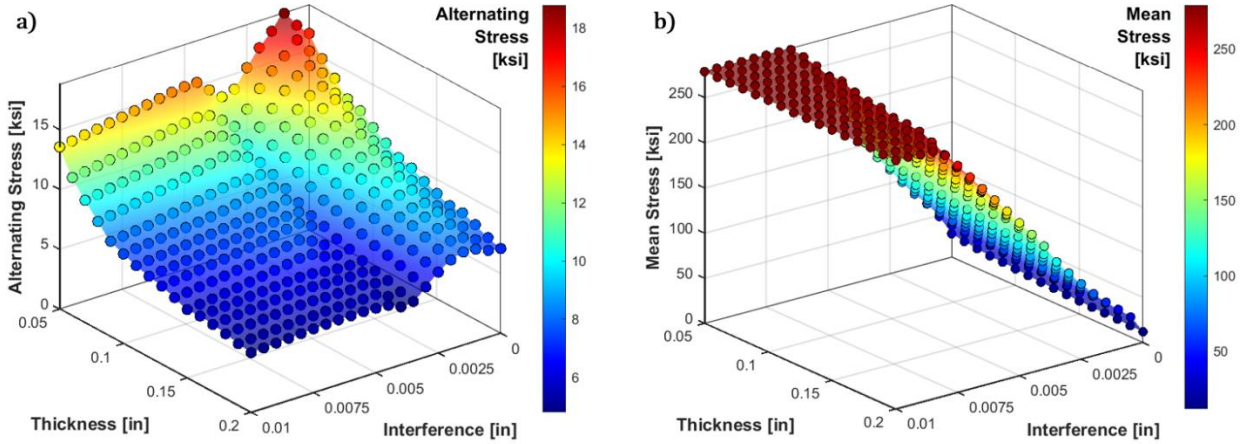


Figure 23. Surface plots of a) alternating stress and b) mean stress versus thickness and interference for 3.33-10 kip loading.

Alternating stress (plotted in Figure 23a) decreases as sleeve thickness increases, but interestingly, it varies with interference. There is a clear peak in alternating stress around 0.0015 in, while there is a dip around an interference of 0.003 in. It is unclear why these peaks are occurring, but it could be due to contact openings or the highest element being extreme. Investigating this further is recommended for future studies. For interferences greater than 0.005 in, the alternating stress is not sensitive to, but does decrease slightly with, increasing interference as seen by the flat lines on the left of Figure 23a. Literature suggests that as interference increases, alternating stress is expected to decrease, which aligns with the trends at interferences greater than 0.005 in [46], [48]. Mean stress (plotted in Figure 23b), on the other

hand, follows a very clear trend: mean stress increases with higher levels of interference and decreases slightly as thickness increases, which aligns with literature [46], [48].

The effect of these variables on fatigue life were subsequently analyzed using the Goodman relation, Equation (1), for each element and then the lowest SF within the sleeve was assigned to that particular geometry. Figure 24a shows the alternating stress and mean stress relationship, overlaid with the Goodman line (SF = 1) for reference. Figure 24b presents the surface plot of fatigue life SF as a function of interference and sleeve thickness.

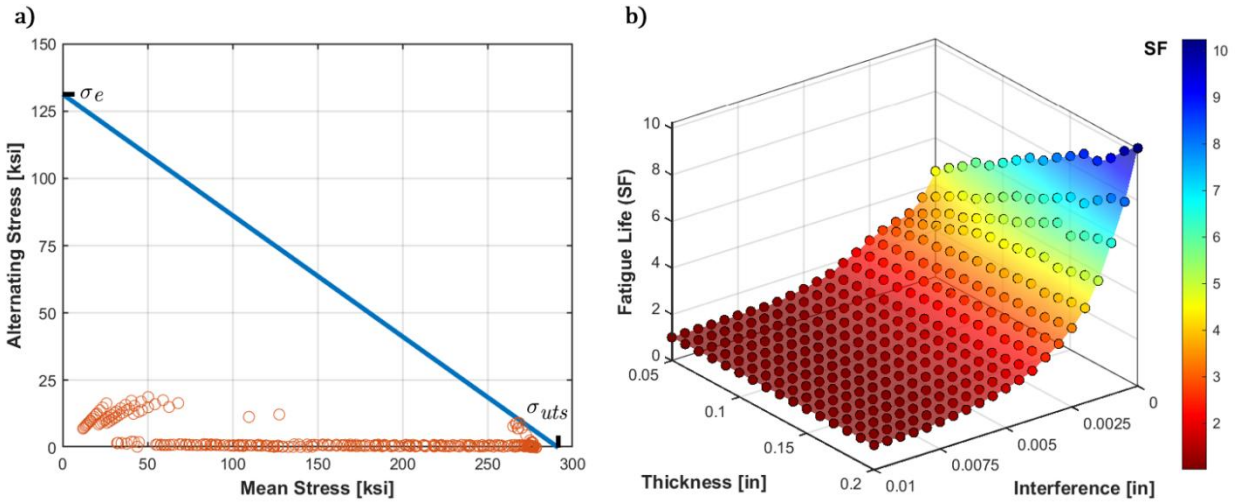


Figure 24. a) Graph of alternating stress versus mean stress with Goodman line and b) surface plot of fatigue life (SF) versus interference and thickness for 3.33-10 kip loading.

Figure 24a highlights that the mean stress appears to be the dominating factor in determining fatigue life according to the Goodman relation rather than the alternating stress. Figure 24b indicates that fatigue life is maximized when interference is minimized, and thickness is maximized. This result is logical, as lower interference reduces mean stress while increased thickness lowers alternating stress, both of which enhance fatigue life performance. Although a low interference increases alternating stress, the results of this loading range (3.33 – 10 kip) indicate that the effect of mean stress on increasing stress outweighs the benefits of increasing

interference to decrease alternating stress when looking at fatigue life SF. However, practical considerations must be made when selecting sleeve geometry. Excessive thickness may not be feasible in all applications, and interference may still provide advantages in joint stiffness and bearing strength [41], [43]. Therefore, based on the parameter ranges of this study, the recommended geometry for a shear sleeve is 0 in interference fit and 0.2 in sleeve thickness.

These results prompt the question: at higher alternating loads, will the alternating stress be more significant and alter the conclusions on fatigue life performance that have been made for this low loading range (3.33 – 10 kip)?

## Parametric Study Results (3.33 – 50 kip)

The parametric study was repeated for the higher load case of 3.33 kip to 50 kip, increasing the load ratio from 1:3 (3.33:10) up to 1:15 (3.33:50). Figure 25a shows alternating stress decreasing with increasing interference and thickness, while Figure 25b shows mean stress increasing with increasing interference, which again matches the literature [46], [48].

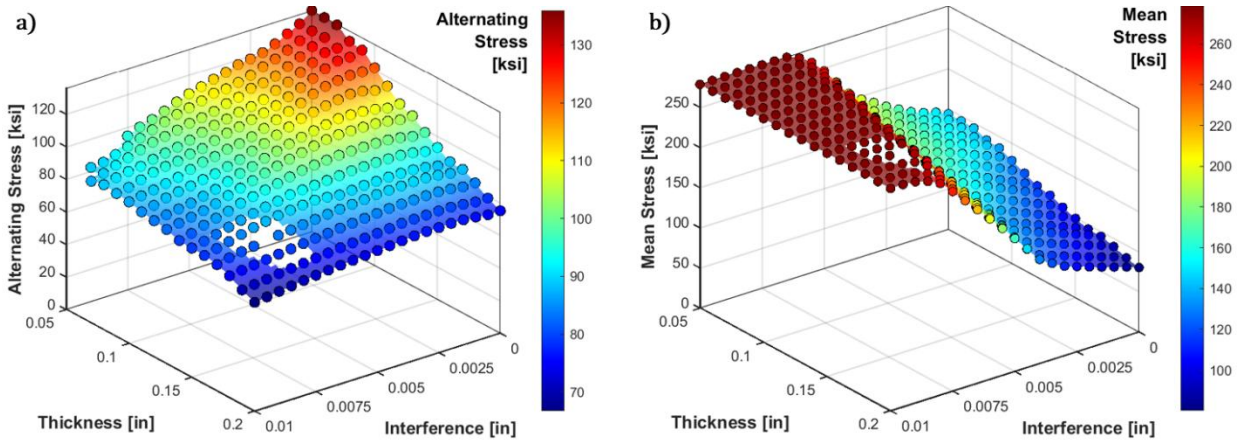


Figure 25. Surface plots of a) alternating stress and b) mean stress versus thickness and interference for 3.33-50 kip loading.

The FE submodel was unable to converge for one geometry (interference = 0.008 in and thickness = 0.17 in) at this higher loading. This missing data point was excluded from the surface plots in Figure 24, however the general trends of the data are still clear.

Fatigue life SF was again evaluated using the Goodman relation and the results are overlaid with the Goodman line (SF = 1) in Figure 26a and on a surface plot in Figure 26b.

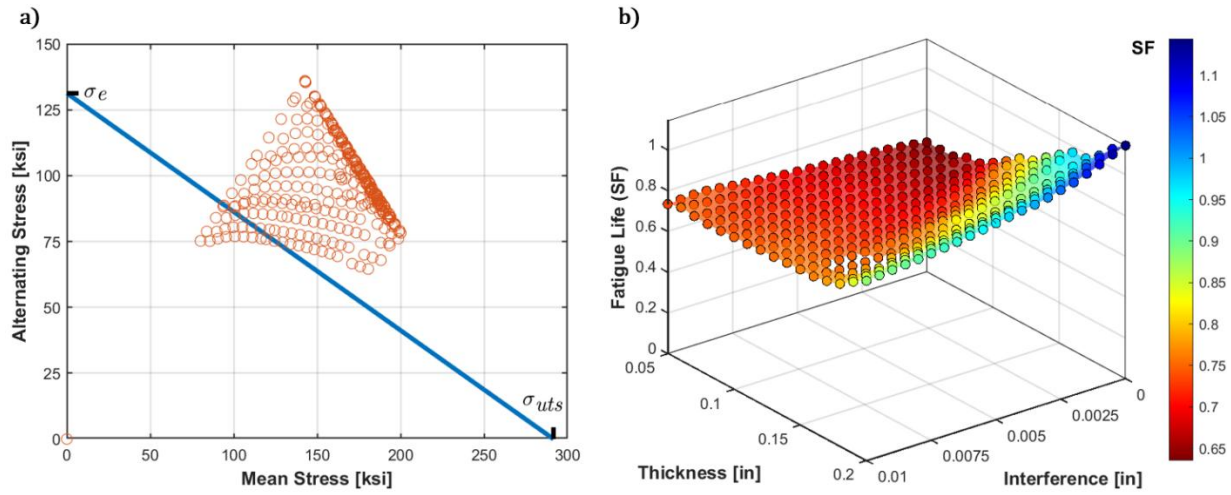


Figure 26. a) Graph of alternating stress versus mean stress with Goodman line and b) surface plot of fatigue life (SF) versus interference and thickness for 3.33-50 kip loading.

Figure 26a shows that the alternating stress components are now presenting a significant impact on fatigue life. Additionally, many of the shear sleeve geometries lie above the Goodman line for this higher loading case, meaning they have a SF < 1 and are not expected to last indefinitely in fatigue. Figure 26b shows a more complex relation than the lower loading case (3.33-10kip). Figure 27 highlights two regions with distinct trends. In Region A, increasing interference improves predicted fatigue life, as the reduction in alternating stress outweighs the increase in mean stress. In contrast, Region B shows that increasing interference reduces predicted fatigue life, as the increase in mean stress surpasses the decrease in alternating stress.

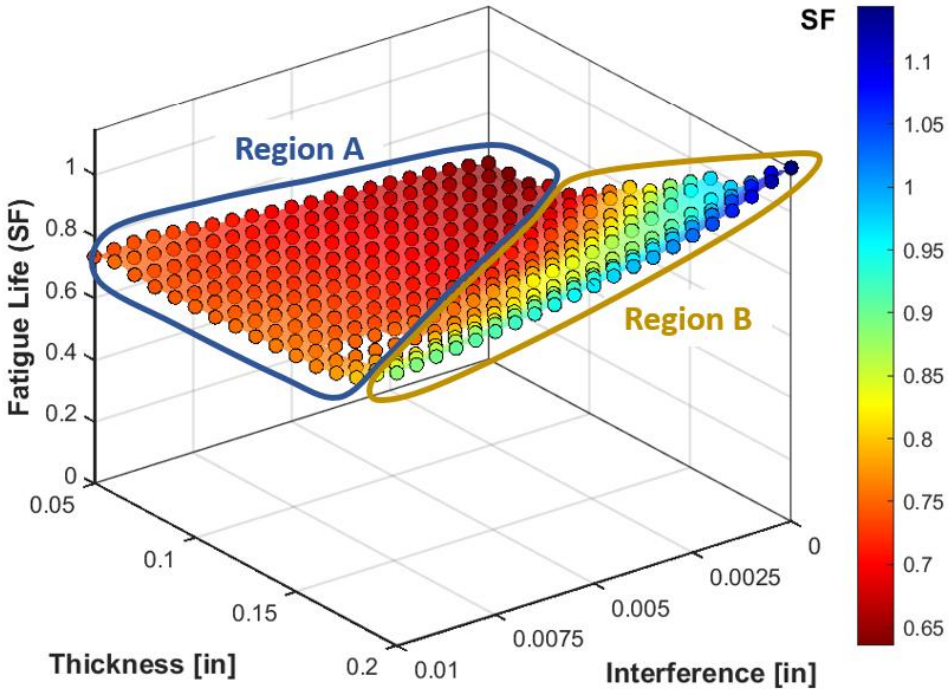


Figure 27. Surface plot of fatigue life (SF) versus interference and thickness for 3.33-50 kip loading. Region A indicates where increasing interference increases SF and Region B indicates where increasing interference decreases SF.

The results of this higher load case reveal a distinct threshold – at the boundary between Region A and Region B – where the effects of interference and thickness on fatigue life SF shift based on the applied load. Future work in this area could focus on evaluating and characterizing this threshold to gain deeper insights into the relationships between interference, sleeve thickness, alternating stress, mean stress and their combined impact on fatigue life.

Ultimately though, for this range of parameters, the recommended sleeve geometry remains at 0 in interference and 0.2 in thickness for optimal fatigue performance.

## Comparison of Load Cases

The impact of applied loading on the relationship between interference, thickness, and stress is highlighted by comparing the 3.33-10 kip and 3.33-50 kip cases. Increasing the applied load leads to a significant rise in alternating stress (Figure 28a), whereas mean stress (Figure 28b) remains relatively unchanged except for cases with very low interference.

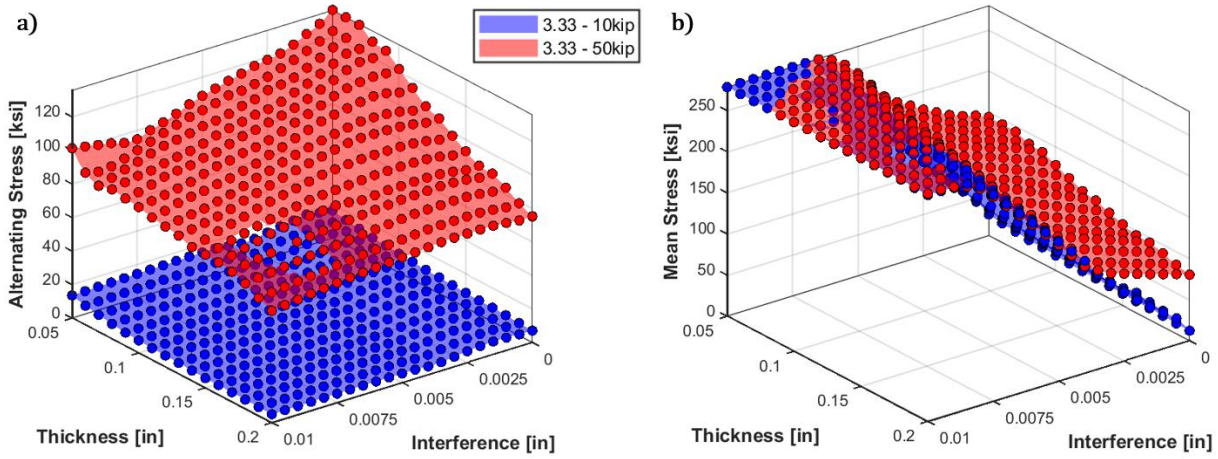


Figure 28. Contour plots comparing a) alternating stress and b) mean stress for both 3.33-10kip (blue) and 3.33-50kip (red)

Figure 28a also shows that increasing the applied stress greatly increases the alternating stress, but increasing interference and thickness are both still effective methods to decrease this alternating stress component. The drastically increased alternating stress is highlighted in Figure 29a by the red data points being much higher on the y-axis than the blue data points.

Figure 29a further demonstrates that increased alternating stress pushes many data points above the Goodman line, indicating eventual failure under fatigue. Figure 29b highlights how fatigue life SF is decreased significantly as applied loading is increased, especially for low interferences.

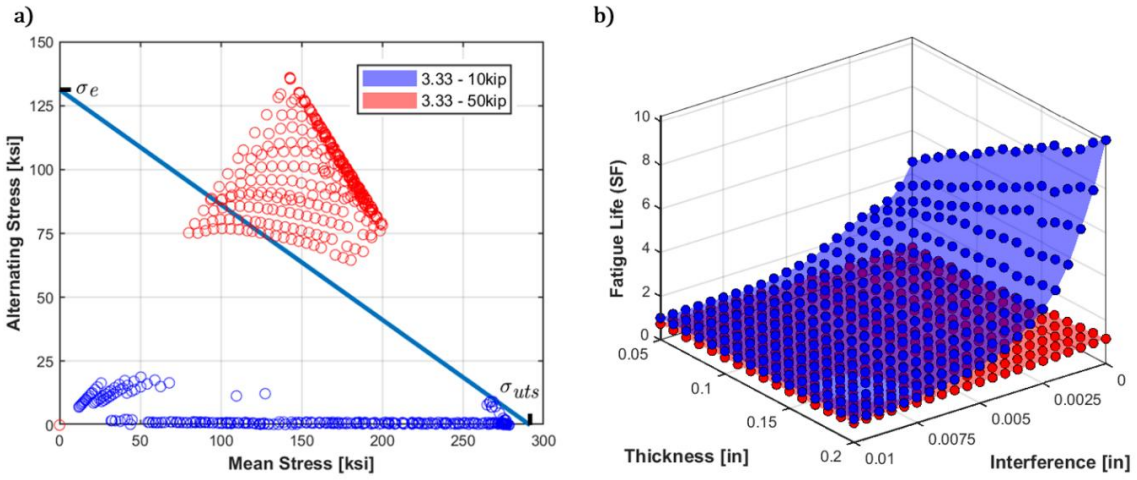


Figure 29. a) Graph of alternating stress versus mean stress with Goodman line and b) surface plot of fatigue life (SF) versus interference and thickness for both 3.33-10 kip (blue) and 3.33-50 kip (red) loading.

The comparison between the two load cases underscores that while both thickness and interference play roles in fatigue life, the level of the applied load amplifies these effects, making shear sleeve optimization more critical at higher loads where failure is possible if the design is poor. Overall, both load cases suggest that optimal shear sleeves will be low interference and high thickness.

# Chapter 4

## Conclusion

The primary goal of this research was to quantity how variations in shear sleeve geometry—specifically interference and thickness—affect the fatigue performance of the sleeve within complex thick composite bolted joints. This was essential for developing optimized designs that could improve the durability and performance of multi-material joints. To achieve this, the study sought to (1) establish a framework for evaluating fatigue in shear sleeves within composite joints, (2) define the design space for parametric exploration, and (3) recommend optimal geometry for enhanced fatigue performance.

The results reveal that both shear sleeve interference and thickness significantly impact alternating and mean stress, which in turn affect fatigue life. At low loads (3.33 – 10 kip), there are notable peaks in alternating stress at small interference values, but once interference exceeds 0.005 in, increasing it reduces alternating stress. This trend is more pronounced at higher loads (3.33 – 50 kip). For each load case, increasing interference is strongly correlated with increasing mean stress. Using the Goodman relation to assess combined stress effects on fatigue life, a threshold emerges beyond which further interference becomes detrimental rather than beneficial to fatigue life. While this threshold was not reached in the low loading case, it was evident in the high loading case, suggesting that load magnitude is crucial in interference-based shear sleeve design. In contrast, increasing thickness consistently reduces both alternating stress and mean stresses, improving fatigue life under both low (3.33-10 kip) and high (3.33-50 kip) loading conditions. These results indicate that while both interference and thickness influence stress behavior, interference has a more complex, load-dependent effect on fatigue life.

Based on the results, the optimal shear sleeve geometry for improved fatigue life would be minimal interference combined with a maximized thickness. For these experiments and parameter range, a 0 in interference and 0.2 in thickness maximized the fatigue life SF. This research contributes to the field by providing a quantifiable understanding of how shear sleeve geometry influences sleeve fatigue life in thick composite joints. Additionally, the methodology developed in this thesis offers a framework for future studies to evaluate joint performance in complex structures and joints. Practically, these findings can inform the design of more durable shear sleeves for use in composite joints for many applications such as aerospace, automotive, marine, construction or defense, where fatigue performance is critical.

To further advance this research, future studies should by conducted to explore different bolt sleeve geometries, load cases and materials to extend the applicability of these findings and should characterize the the threshold of when interference improves fatigue life versus reducing it. Additionally, future studies should investigate the effect that interference has on alternating stress for low load cases. Incorporating additional parameters such as varying load ratios, bolt sizes and temperature effects could provide a more comprehensive understanding of shear sleeve fatigue behavior in composite joints. Since this study only focused on fatigue life of the metal shear sleeve, there is significant potential for characterizing the fatigue life of the composite itself.

In conclusion, this study has provided a framework for optimizing shear sleeve geometry to enhance fatigue life in sleeves within thick composite joints. By offering practical design recommendations and identifying avenues for future research, this work contributes to improving joint fatigue performance in bolted, thick composite joints.

## Appendix A: Modeling interference fits

To build confidence in modeling interferences in more complex joints, a simple FE model was developed to match closed-form solutions for interference fits. In these solutions, stress is separated into radial and tangential components based on the applied pressure ($p$), as illustrated in Figure A.1 [64].

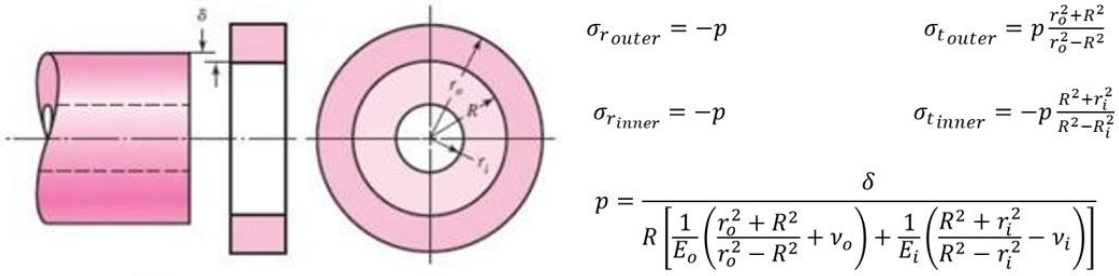


Figure A.1. Interference fit calculations. Modified with permission from [64].

For this simplified example, the model involves two sleeves with a 1% interference. The geometry and material properties of the sleeves are summarized in Table A.1. An FE model was constructed to simulate this interference fit.

**Table A.1 Material properties and geometry of sleeves**

| Part | Material | Modulus of Elasticity ($E$) [ksi] | Poisson's Ratio ($\nu$) | Inner Radius [in] | Outer Radius [in] |
|---|---|---|---|---|---|
| Inner Sleeve | Steel | 30,000 | 0.3 | 3 | 5.05 |
| Outer Sleeve | NAB | 17,000 | 0.34 | 5 | 25 |

The interference was applied between the outer diameter (OD) of the inner sleeve and the inner diameter (ID) of the outer sleeve. Additionally, the interference fit option "gradually remove secondary node overclosure during this step" was selected to ensure accurate contact during the simulation. To reduce computational time, symmetry boundary conditions were applied in both the X and Y directions. A local coordinate system $(r, \theta, z)$ was introduced to

analyze the radial and tangential stress components. Figure A.2 provides a visualization of the results, and Figure A.3 shows the calculations that were compared to the closed-form solutions.

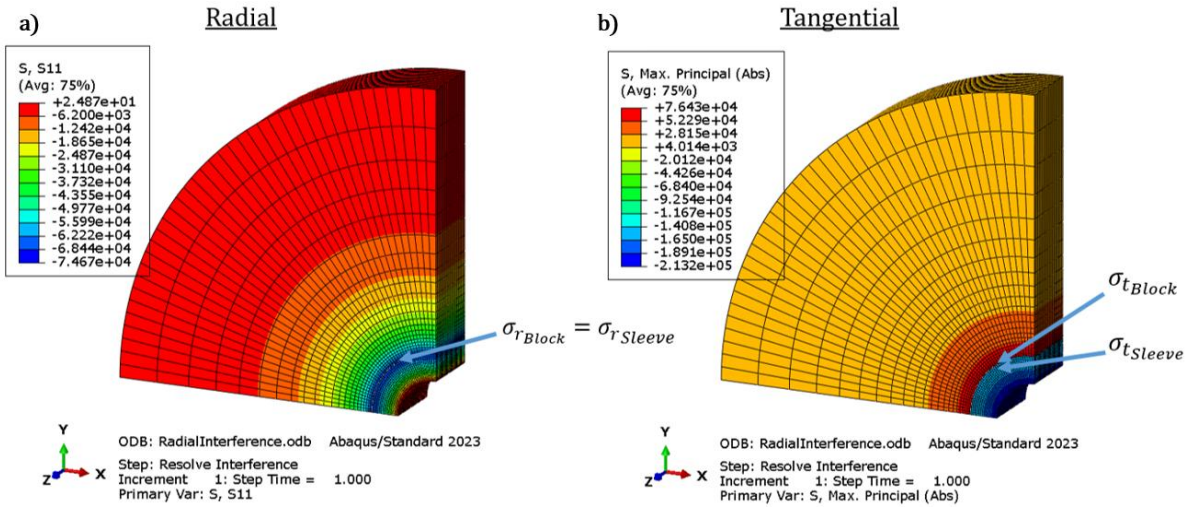


Figure A.2. Visual display of a) radial stress ($\sigma_r$) and b) tangential stress ($\sigma_t$) in sleeves.

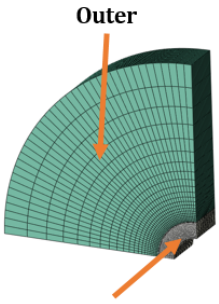


*FEA results are stress averages of elements on ID of Outer Cylinder and OD of Inner Cylinder*

| | **$S_{11}$ – Radial** | **Max Principal (Abs) – Tangential** |
|---|---|---|
| | $\sigma_{Outer_{FEA}} = -68.2\ ksi$<br>$\sigma_{Outer_{calc}} = -69.2\ ksi$ | $\sigma_{Outer_{FEA}} = 74.1\ ksi$<br>$\sigma_{Outer_{calc}} = 75.0\ ksi$ |
| | % Error = 1.44% | % Error = 1.20% |
| | $\sigma_{Inner_{FEA}} = -67.8\ ksi$<br>$\sigma_{Inner_{calc}} = -69.2\ ksi$ | $\sigma_{Inner_{FEA}} = -145\ ksi$<br>$\sigma_{Inner_{calc}} = -147\ ksi$ |
| | % Error = 2.02% | % Error = 1.36% |

**All errors are ≤ 2%, indicating that the FE model accurately represents the interference-fit**

Figure A.3. Comparison of FEA results with closed-form solutions for $\sigma_r$ and $\sigma_t$. The margin of error is approximately ≤ 2%, demonstrating that the FE model accurately captures the interference fit behavior.

The results from this simple FE model indicate that the interference modeling technique accurately represents the stress response due to an interference fit, correlating well with the closed-form solution. This modeling technique will be consistently used in all interference fits simulations throughout this thesis.

## Appendix B: Modeling thick, bolted CFRPs under bending loads

To further validate the accuracy of complex bolted joint modeling, the experiments conducted by Gorjipoor et al. were replicated in this appendix [12], [13]. Gorjipoor et al. developed an FE model in ANSYS and conducted experimental testing using digital image collection (DIC) for both a cross-ply and unidirectional layup subjected to cantilever bending forces [13]. In this appendix, an Abaqus model was created to match their model. Figure B.1 compares the FE models: Gorjipoor et al.'s model in ANSYS and the recreated model in Abaqus.

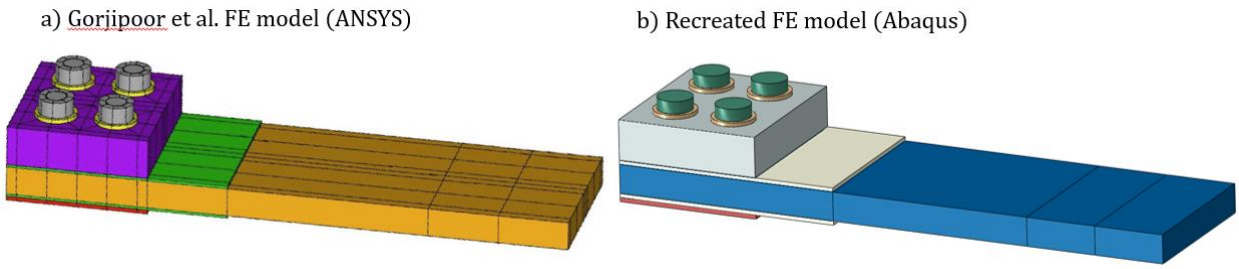


Figure B.1. Comparison of FE models: a) Gorjipoor et al.'s ANSYS model & b) recreated Abaqus model

The Abaqus model was developed based on the description, dimensions, material properties, contacts, boundary conditions and mesh detailed in Gojipoor et al.'s paper [13]. Figure B.2. illustrates the strain correlation between each model and the experimental results.

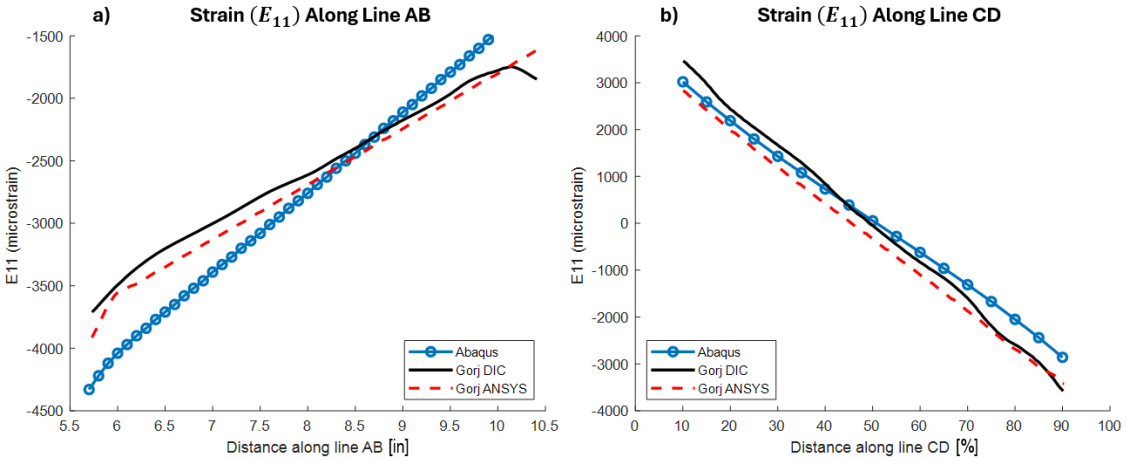


Figure B.2. Comparison of strain data from the recreated Abaqus model, DIC results and ANSYS model for a) $E_{11}$ along Line AB and b) $E_{11}$ along Line CD.

For the cross-ply layup, the slope of Line AB was not ideal, but the correlation with $E_{11}$ along Line CD was not ideal. During further investigation of this study, discrepancies in their data were identified. For the cross-ply layup, the results for $E_{13}$ along Line EF differed from the recreated model's results. A deeper analysis revealed that the coordinates for Line EF in their data were not consistent with those previously stated. They reported the maximum value at 68% along Line EF, but their graph in Figure B.3a indicated the maximum occurred at ~45%. Additionally, their z-coordinate in Table 7 of Gorjipoor et al.'s paper differed from the original indication of Line EF's location. By flipping and shifting the collected data so that the maximum occurred at ~45% along the adjusted line, the trends become more similar, as shown in Figure B.3b.

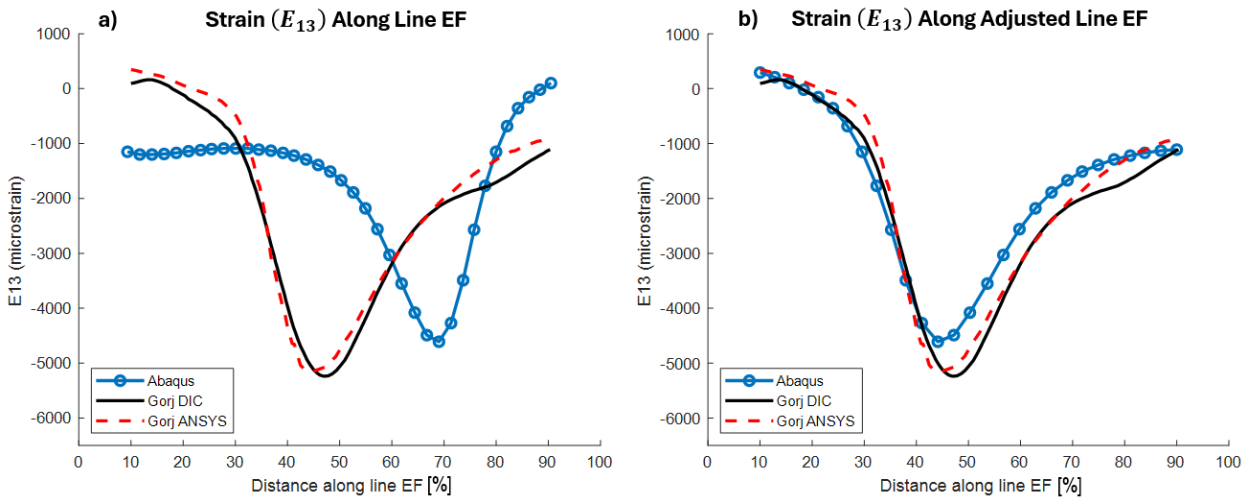


Figure B.3. Graphs of $E_{13}$ strain data along Line EF from the recreated Abaqus model, DIC results and ANSYS model. Graph a) shows the unadjusted Line EF data, while graph b) shows a strong correlation for adjusted Line EF.

For the unidirectional layup results, the correlation followed a similar pattern to the cross-ply results across all three plots, assuming the same data flipping and transformation for Line EF as shown in Figure B.4.

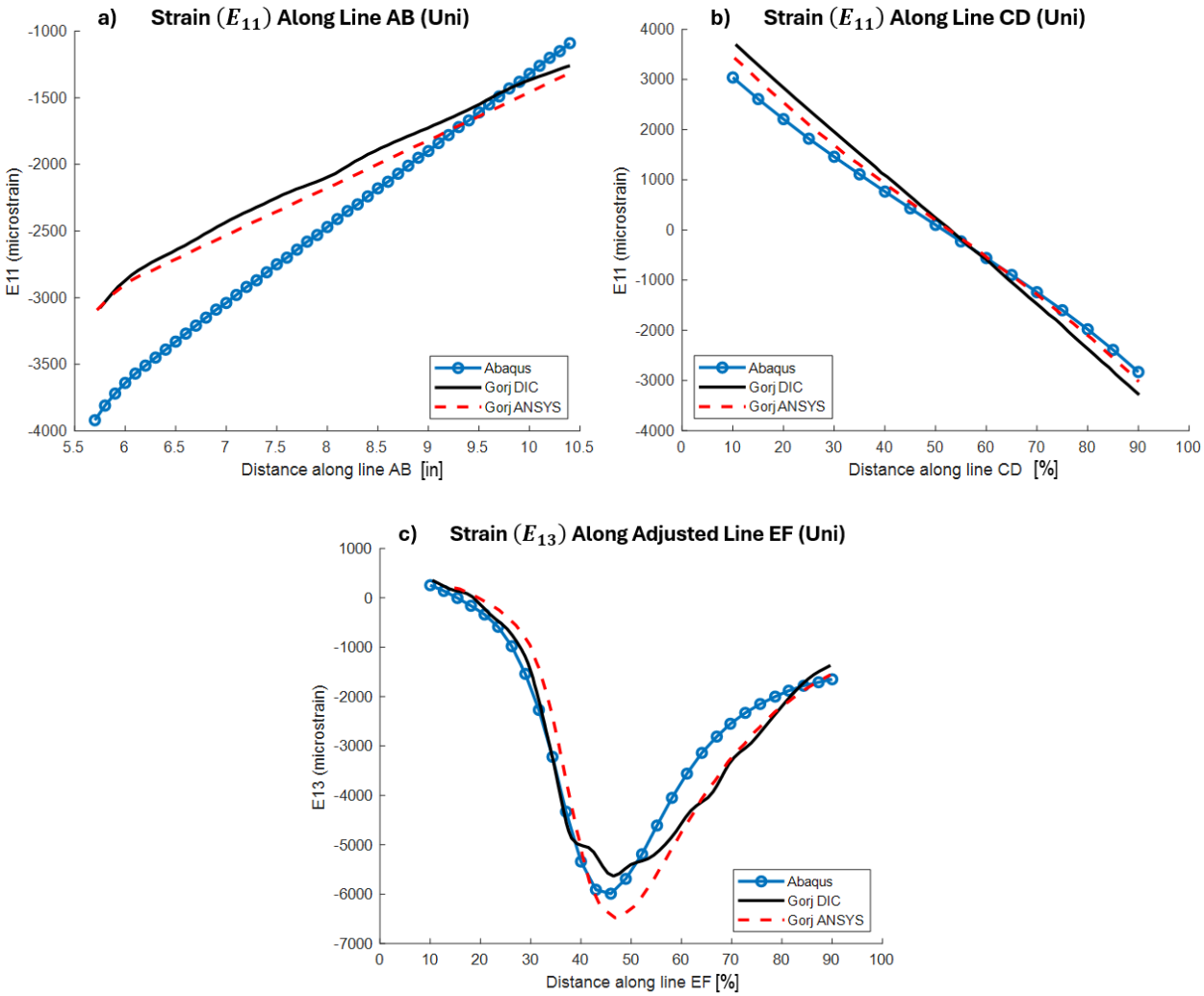


Figure B.4. Comparison of strain data from the recreated Abaqus model, DIC results and ANSYS model for a) $E_{11}$ along Line AB, b) $E_{11}$ along Line CD, and c) $E_{13}$ along the adjusted Line EF.

Overall, the strong correlation in strain data trends between the Abaqus model and the ANSYS model, as well as the experimental DIC demonstrate that the Abaqus FE model accurately captures the physical behavior of the composite [13]. Given that Gorjipoor et al.'s experiment closely mirrors the setup used in this thesis—a thick bolted composite in bending—this strong correlation supports the assumption that the model correctly captures the complex bolted joint under investigation.

## Appendix C: Submodeling and parametric sweeps

This appendix describes the submodeling process and the development of the Python code for conducting parametric sweeps involving geometry changes. Both the global model and submodel were created in Abaqus CAE 2023, following a YouTube tutorial by Ahmed Elkady [67]. Initially, the global model was created, followed by the addition of partitions to delineate the submodel's location. Material properties, boundary conditions, loading steps, and a coarse mesh were established. The global model was then duplicated and renamed to "Model-Submodel." All cells outside the designated submodel region were deleted, leaving only the submodel region as shown in Figure C.1.

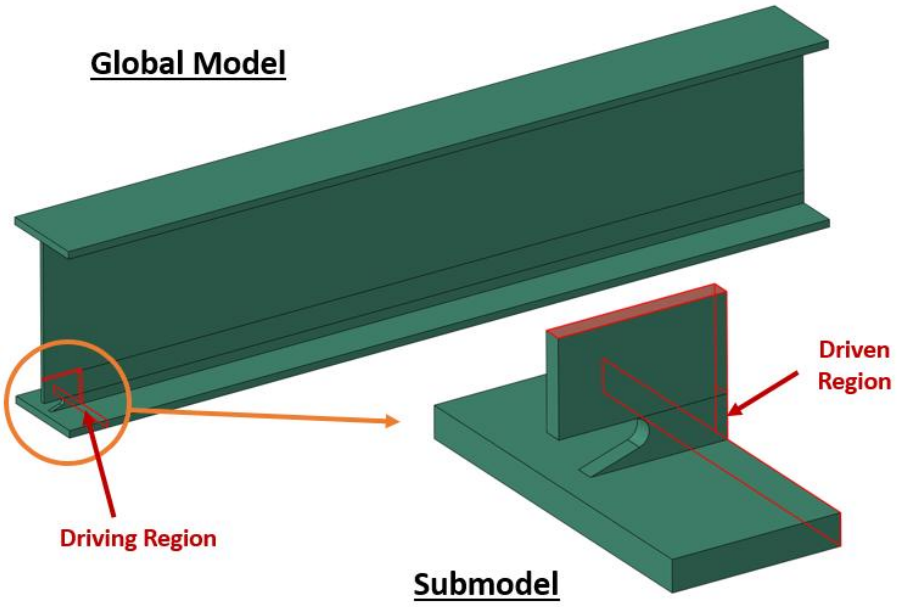


Figure C.1. Diagram of submodel from the global model for a simple beam with driving and driven regions highlighted.

A set named "driven_region" was defined on the surfaces of the submodel that interface with the global model. Likewise, a set named "driving_region" was defined within the Model-Global on the surfaces of the partitions that outline the edges of the submodel. Once these sets

were established, a submodel boundary condition was created within the Model-Submodel, using the “Other” category in Abaqus to specify the driven region and driving region, as shown in Figure C.2a.

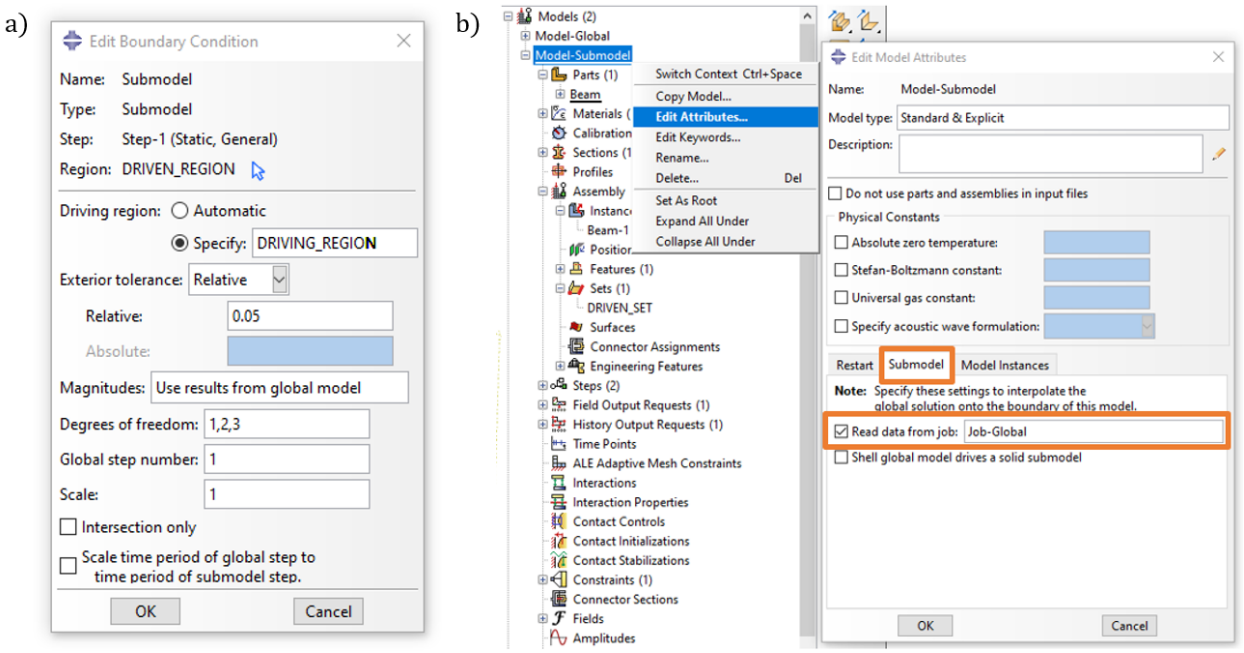


Figure C.2. Screenshot of a) submodel boundary condition and b) linking with global model.

After fully defining the global model and creating the necessary sets, a job named “Job-Global” executed. Upon completion, the output database “Job-Global.odb” was referenced by the submodel by editing the attributes of Model-Submodel, as depicted in Figure C.2b. This linkage between the global and submodel allows the submodel to be run and geometry changes to be made within it.

Abaqus automatically generates .jnl files that log changes made to the .cae file in Python format, which is instrumental for script development [63]. To create a script capable of iterating through geometry changes for this submodel, the necessary manual edits were first performed, and the corresponding lines from the .jnl file were copied and incorporated into a loop.

Additionally, it was essential to import the necessary Abaqus modules and establish a job naming convention to prevent overwriting of previous jobs. Using the code provided at the end of this appendix, three jobs with varying notch sizes were successfully created and executed by navigating to File > Run Script > Submodel.py. The results, displayed in Figure C.3, confirm successful geometry iteration and changes in stress contours.

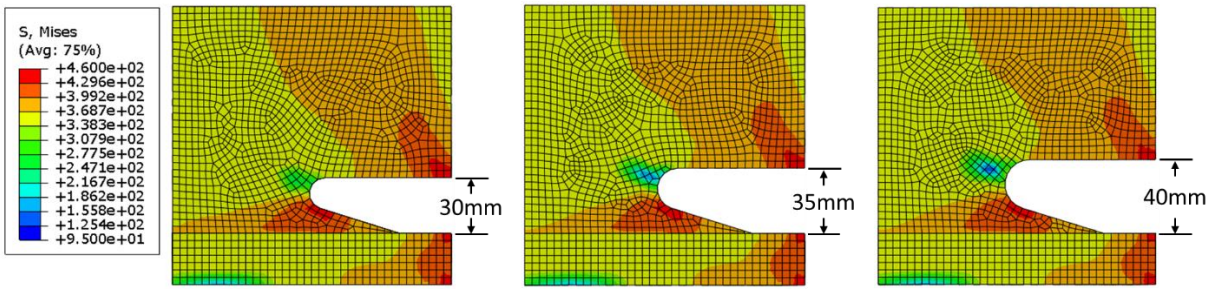


Figure C.3. Results from a simple parametric study on the effect of cutout size (ranging from 30 - 40 mm) on Von Mises Stress contours.

The methodologies described in this appendix represent a progression in the use of Abaqus and Python, building confidence in the final experiment and its results. This work serves as a foundation for more complex submodeling applications in the main experiments of this thesis.

```
# Submodel.py       Developed by: Luke Jeffery
# This code loops through cutout sizes in a beam within a submodel.

from part import *
from material import *
from section import *
from assembly import *
from step import *
from interaction import *
from load import *
from mesh import *
from optimization import *
from job import *
from sketch import *
from visualization import *
```

```
from connectorBehavior import *
from sys import *
from array import *
from odbAccess import *

# Define Variables
run = 0
runJobs = True
sizeMax = 40.0  # [mm]
sizeMin = 30.0  # [mm]
sizeStep = 5.0  # [mm]
size = sizeMin

print('Starting parametric study \n') # write out info to the Abaqus command area

# Loop Through Cutout Sizes
for i in range (int((sizeMax - sizeMin)/sizeStep)+1):
    if run > 0:
        size += sizeStep
        run += 1

    # Name Job
    jobName = 'Job_{:04}'.format(run)  # define string "jobName" with job number
    fullJobName = jobName + '.odb'
    print(jobName + '   Starting Run # ' + str(run) + ' of ' +
        str(int((sizeMax - sizeMin)/sizeStep)+1) + '\n')

    # Edit Geometry
    mdb.models['Model-Submodel'].ConstrainedSketch(name='__edit__',
        objectToCopy=mdb.models['Model-Submodel'].parts['Beam'].features['Cut
        extrude1'].sketch)
    mdb.models['ModelSubmodel'].parts['Beam'].projectReferencesOntoSketch(filter=
        COPLANAR_EDGES, sketch=mdb.models['Model-Submodel'].sketches['__edit__'],
        upToFeature=mdb.models['Model-Submodel'].parts['Beam'].features['Cut
        extrude-1'])
    # Adjust the size of the cutout
    mdb.models['Model-Submodel'].sketches['__edit__'].dimensions[2].setValues(
        value=size)
    mdb.models['Model-Submodel'].sketches['__edit__'].dimensions[3].setValues(
        value=(size/2)-6.5)
    mdb.models['Model-Submodel'].parts['Beam'].features['Cut extrude-1'].setValues(
        sketch=mdb.models['Model-Submodel'].sketches['__edit__'])
    del mdb.models['Model-Submodel'].sketches['__edit__']
    mdb.models['Model-Submodel'].parts['Beam'].regenerate()
    mdb.models['Model-Submodel'].rootAssembly.regenerate()
    mdb.models['Model-Submodel'].parts['Beam'].generateMesh()

    # Create and Submit Job
    if runJobs:
        myJob = mdb.Job(atTime=None,contactPrint=OFF,description='Cutout Size = '
```

```
            + str(size), echoPrint=OFF, explicitPrecision=SINGLE,
            getMemoryFromAnalysis=True, historyPrint=OFF, memory=90,
            memoryUnits=PERCENTAGE, model='Model-Submodel', modelPrint=OFF,
            multiprocessingMode=DEFAULT, name=jobName, nodalOutputPrecision=SINGLE,
            numCpus=4, numGPUs=0, numThreadsPerMpiProcess=1, queue=None,
            resultsFormat=ODB, scratch='', type=ANALYSIS, userSubroutine='',waitHours=0,
            waitMinutes=0)
        myJob.submit()
        myJob.waitForCompletion()

print('All Iterations Successfully Completed')
```

## Appendix D: Parametric sweeps Python code

```
'''
The purpose of this code is to create the .inp files for a parametric sweep to
investigate the effects of interference fit and shear sleeve thickness on fatigue
life. This code is to be run using the run script function within Abaqus in the
developed Global_Model.cea file

Developed by Luke Jeffery using base code structure developed by Will Carsky
'''

from part import *
from material import *
from section import *
from assembly import *
from step import *
from interaction import *
from load import *
from mesh import *
from optimization import *
from job import *
from sketch import *
from visualization import *
from connectorBehavior import *
from sys import * #add this line to allow writing to Abaqus command window
from array import *
from odbAccess import *

# Define post processing functions

# Extracts element stress data from a step and instance of a .odb file
def extractStressData(odbName, stepName, instance):
    stressData = []
    odb = openOdb(odbName)
    instance = odb.rootAssembly.instances[instance]
    step = odb.steps[stepName] # Troubleshooting: print(odb.steps)
    frame = step.frames[-1] # Get the last frame
    stressSet = frame.fieldOutputs['S'].getSubset(position=CENTROID) # S = stress
    for stressValue in stressSet.values:
        if stressValue.instance == instance:
            elementID = stressValue.elementLabel # Get element ID
            vonMisesStress = stressValue.mises # Get Mises Stress
            stressData.append([elementID, vonMisesStress])
    odb.close()
    return stressData

# Calculates a SF using the Goodman relation
def getFatigueLife (odbName):
    # Extract stress data for the steps we're oscillating between
    try:
```

```
stressData50 = extractStressData(odbName, 'Compression 3p33 kips', 'Sleeve B')
stressData150 = extractStressData(odbName, 'Compression 10 kips', 'Sleeve B')

jobName = odbName.split(".")[0] # remove the .odb from odbName string
fout = open(str('' + jobName + '.txt'), 'w')  # create file for results

# Store stress data from each step in one array
combinedStressData = []
S_uts = 291671 # [psi] Ultimate tensile strength [or 2011 MPa]
S_end = 125443 # [psi] Endurance limit [or 864.9 MPa)
min_SF = 100
min_SF_Element = 0
min_alt = 0
min_mean = 0
max_alt = 0
max_mean = 0

# Apply Goodman relation to find
for data50, data150 in zip(stressData50, stressData150):
    elementID50, mises50 = data50
    elementID150, mises150 = data150

    S_alt = abs(mises150 - mises50)/2     # [psi]
    S_mean = abs(mises150 + mises50)/2    # [psi]
    SF = 1/((S_alt/S_end)+(S_mean/S_uts)) # [psi]
    if SF < min_SF:
        min_SF = SF
        min_SF_Element = elementID50
        min_alt = S_alt
        min_mean = S_mean

    if S_alt > max_alt:
        max_alt = S_alt

    if S_mean > max_mean:
        max_mean = S_mean

    # Record Stress Data
    if elementID50 == elementID150:
        combinedStressData.append([elementID50, mises50, mises150, S_alt, S_mean,
        SF, max_alt, max_mean])
    else:
        print('ELEMENT IDs ARE CHANGING!')

    # Write out job name and job results to file
    fout.write(str(elementID50) + '\t' + str(mises50) + '\t' + str(mises150) +
        '\t' + str(min_alt) + '\t' + str(min_mean) + '\t' + str(SF) + '\t' +
        str(max_alt) + '\t' + str(max_mean) + '\n')

# If the job fails for any reason
except Exception as e:
```

```
            print('Job_{:04} failed: {}'.format(run, str(e)))
            combinedStressData = []
            min_SF = 0
            min_SF_Element = 0
            min_alt = 0
            min_mean = 0
            max_alt = 0
            max_mean = 0

    return combinedStressData, min_SF, min_SF_Element, min_alt, min_mean, max_alt,
        max_mean

############################### Main Script ################################

# getFatigueLife('Job-Global-03.odb')
# Comment out everything below if you want to just post process for a single job

# Define variables
interferenceMin = 0       # [in], 0.0015 was original
interferenceMax = 0.0101       # [in]
interferenceStep = 0.0005      # 21 times
interference = interferenceMin
thicknessMin = 0.05      # [in], 0.172 was original
thicknessMax = 0.2       # [in]
thicknessStep = 0.01     #16 times
thickness = thicknessMin
geometryUpdated = False

sleeveIR = 0.328 # [in] this is a constant for this research study
run = 0
holeIR = 0
sleeveOR = 0
modifyGeometry = False
runJobs = False
postProcess = True
totalJobCount = int((interferenceMax-interferenceMin)/interferenceStep+1) *
    int((thicknessMax-thicknessMin)/thicknessStep+1)

# Create and open a file for results
fout = open('Results_Fine_Mesh_' + str(totalJobCount) + '_3p33_10.txt', 'w')
print('Starting parametric study \n') # write out info to the Abaqus command area

for i in range(int((interferenceMax-interferenceMin)/interferenceStep+1)):
    print('Interference iteration: ' + str(i+1) + '\n')
    interference = interferenceMin + interferenceStep * i # diameter interference

    for t in range(int((thicknessMax-thicknessMin)/thicknessStep+1)):
        print('Thickness iteration: ' + str(t+1) + '\n')
        thickness = thicknessMin + thicknessStep * t
        run += 1
```

```
# Name jobs with interference & thickness (decimals with p)
jobName = 'Job_Int_{}_Thk_{}'.format(str(interference).replace('.', 'p'),
    str(thickness).replace('.', 'p'))
fullJobName = jobName + '.odb'
print(jobName + '\tStarting Run #' + str(run) + ' of ' + str(totalJobCount) +
    '\tInterference: '+str(interference)+ '\tThickness: '+str(thickness) +'\n')
#print(jobName)
holeIR = sleeveIR + thickness # [in]
sleeveOR = sleeveIR + thickness + (interference/2) # [in]
print('\tHole Inner Radius: ' + str(holeIR) + '\tSleeve Outer Radius: ' +
    str(sleeveOR) + '\n')

if modifyGeometry:
    try:
        # Edit Beam hole geometry & partition
        mdb.models['Model-Submodel'].parts['Beam'].deleteMesh()
        mdb.models['Model-Submodel'].ConstrainedSketch(name='__edit__',
            objectToCopy=mdb.models['Model-Submodel'].parts['Beam'].features['Cut
            extrude-1'].sketch)
        mdb.models['Model-Submodel'].parts['Beam'].projectReferencesOntoSketch(
            filter=COPLANAR_EDGES, sketch=
        mdb.models['Model-Submodel'].sketches['__edit__'], upToFeature=
            mdb.models['Model-Submodel'].parts['Beam'].features['Cut extrude-1'])
        mdb.models['Model-Submodel'].sketches['__edit__'].dimensions[7].setValues
            (value=holeIR)
        mdb.models['Model-Submodel'].parts['Beam'].features['Cut extrude-
            1'].setValues(sketch=mdb.models['Model-Submodel'].sketches[
            '__edit__'])
        del mdb.models['Model-Submodel'].sketches['__edit__']
        mdb.models['Model-Submodel'].ConstrainedSketch(name='__edit__',
            objectToCopy=mdb.models['Model-Submodel'].parts['Beam'].features[
            'Shell extrude-1'].sketch)
        mdb.models['Model-Submodel'].parts['Beam'].projectReferencesOntoSketch(
            filter=COPLANAR_EDGES, sketch=mdb.models['Model-Submodel'].sketches[
            '__edit__'], upToFeature=mdb.models['Model-Submodel'].parts['Beam'].
            features['Shell extrude-1'])
        mdb.models['Model-Submodel'].sketches['__edit__'].dimensions[1].
            setValues(value=holeIR + 0.145) # partition is 0.145in from hole
        mdb.models['Model-Submodel'].parts['Beam'].features['Shell extrude-
            1'].setValues(sketch=mdb.models['Model-Submodel'].sketches[
            '__edit__'])
        del mdb.models['Model-Submodel'].sketches['__edit__']
        mdb.models['Model-Submodel'].parts['Beam'].regenerate()
        mdb.models['Model-Submodel'].parts['Beam'].generateMesh()

        # Edit palm block hole geometry (they're imported as parasolids)
        # Palm Block Bottom
        mdb.models['Model-Submodel'].parts['Palm Block_Bottom'].deleteMesh()
        mdb.models['Model-Submodel'].ConstrainedSketch(name='__edit__',
            objectToCopy=mdb.models['Model-Submodel'].parts['Palm
            Block_Bottom'].features['Cut extrude-3'].sketch)
```

```
mdb.models['Model-Submodel'].parts['Palm
    Block_Bottom'].projectReferencesOntoSketch(filter=COPLANAR_EDGES,
    sketch=mdb.models['Model-Submodel'].sketches['__edit__'],
    upToFeature=mdb.models['Model-Submodel'].parts['Palm
    Block_Bottom'].features['Cut extrude-3'])
mdb.models['Model-Submodel'].sketches['__edit__'].dimensions[0].
    setValues(value=holeIR)
mdb.models['Model-Submodel'].parts['Palm Block_Bottom'].features['Cut
    extrude-3'].setValues(sketch=mdb.models['Model-Submodel'].sketches[
    '__edit__'])
del mdb.models['Model-Submodel'].sketches['__edit__']
mdb.models['Model-Submodel'].parts['Palm Block_Bottom'].regenerate()
mdb.models['Model-Submodel'].parts['Palm Block_Bottom'].generateMesh()

# Palm Block Top
mdb.models['Model-Submodel'].parts['Palm Block_Top'].deleteMesh()
mdb.models['Model-Submodel'].ConstrainedSketch(name='__edit__',
    objectToCopy=mdb.models['Model-Submodel'].parts['Palm
    Block_Top'].features['Shell extrude-3'].sketch)
mdb.models['Model-Submodel'].parts['Palm Block_Top'].
    projectReferencesOntoSketch(filter=COPLANAR_EDGES, sketch=
    mdb.models['Model-Submodel'].sketches['__edit__'], upToFeature=
    mdb.models['Model-Submodel'].parts['Palm Block_Top'].features['Shell
    extrude-3'])
mdb.models['Model-
    Submodel'].sketches['__edit__'].dimensions[0].setValues(value=holeIR)
mdb.models['Model-Submodel'].parts['Palm Block_Top'].features['Shell
    extrude-3'].setValues(sketch=mdb.models['Model-Submodel'].sketches[
    '__edit__'])
del mdb.models['Model-Submodel'].sketches['__edit__']
mdb.models['Model-Submodel'].parts['Palm Block_Top'].regenerate()
mdb.models['Model-Submodel'].parts['Palm Block_Top'].generateMesh()

# Edit Shear Sleeve geometry
mdb.models['Model-Submodel'].parts['Shear Sleeve_noFlats'].deleteMesh()
mdb.models['Model-Submodel'].ConstrainedSketch(name='__edit__',
    objectToCopy=mdb.models['Model-Submodel'].parts['Shear
    Sleeve_noFlats'].features['Solid extrude-1'].sketch)
mdb.models['Model-Submodel'].parts['Shear Sleeve_noFlats'].
    projectReferencesOntoSketch(filter=COPLANAR_EDGES, sketch=
    mdb.models['Model-Submodel'].sketches['__edit__'], upToFeature=
    mdb.models['Model-Submodel'].parts['Shear Sleeve_noFlats'].
    features['Solid extrude-1'])
mdb.models['Model-Submodel'].sketches['__edit__'].dimensions[0].
    setValues(value=sleeveOR)
mdb.models['Model-Submodel'].parts['Shear Sleeve_noFlats'].features[
    'Solid extrude-1'].setValues(sketch=mdb.models['Model-Submodel'].
    sketches['__edit__'])
del mdb.models['Model-Submodel'].sketches['__edit__']
mdb.models['Model-Submodel'].parts['Shear Sleeve_noFlats'].regenerate()
mdb.models['Model-Submodel'].parts['Shear Sleeve_noFlats'].
```

```
                generateMesh()

            # Create Jobs & .inp files
            myJob = mdb.Job(atTime=None, contactPrint=OFF, description= 'Geometry:
                Interference = ' + str(interference) + '   Thickness = ' +
                str(thickness), echoPrint=OFF, explicitPrecision=SINGLE,
                getMemoryFromAnalysis=True, historyPrint=OFF, memory=90,
                memoryUnits=PERCENTAGE, model='Model-Submodel', modelPrint=OFF,
                multiprocessingMode=DEFAULT, name=jobName,
                nodalOutputPrecision=SINGLE, numCpus=4, numGPUs=0,
                numThreadsPerMpiProcess=1, numDomains=4, queue=None,
                resultsFormat=ODB, scratch='', type=ANALYSIS, userSubroutine='',
                waitHours=0, waitMinutes=0)

            myJob.writeInput(consistencyChecking=OFF)
            geometryUpdated = True

        # If the job fails for any reason
            except Exception as e:
                print('Job_{:04} failed: {}'.format(run, str(e)))
                geometryUpdated = False

    # Run Jobs
    if runJobs and geometryUpdated:
        myJob.submit()
        myJob.waitForCompletion()

    if postProcess:
        [combinedStressData,SF_min,element_min,alt_min,mean_min,alt_max,mean_max] =
            getFatigueLife(fullJobName)

        # Writing to file
        fout.write(str(interference) + '\t' + str(thickness) + '\t' + str(alt_min) +
            '\t' + str(mean_min) + '\t' + str(SF_min) + '\t' + str(alt_max) + '\t' +
            str(mean_max) + '\n')

        # Write out job name and results to Abaqus command line
        print('Job_{:04}'.format(run) + '\t' + str(interference) + '\t' +
            str(thickness) + '\t' + str(alt_min) + '\t' + str(mean_min) + '\t' +
            str(SF_min) + '\t' + str(alt_max) + '\t' + str(mean_max) + '\n')

fout.close()
print('All Iterations Successfully Completed!')
```

# BIBLIOGRAPHY

[1] W. Nsengiyumva, S. Zhong, J. Lin, Q. Zhang, J. Zhong, and Y. Huang, "Advances, limitations and prospects of nondestructive testing and evaluation of thick composites and sandwich structures: A state-of-the-art review," Jan. 15, 2021, *Elsevier Ltd*. doi: 10.1016/j.compstruct.2020.112951.

[2] Miracle Daniel and S. Donaldson, *ASM Handbook*, vol. 21. Materials Park: ASM International, 2001.

[3] H. Chebbi and D. Prémel, "The fast computation of eddy current distribution and probe response in homogenized composite material based on semi-analytical approach," *EPJ Applied Physics*, vol. 89, no. 1, Jan. 2020, doi: 10.1051/EPJAP/2020190220.

[4] D. Abliz, Y. Duan, L. Steuernagel, L. Xie, D. Li, and G. Ziegmann, "Curing Methods for Advanced Polymer Composites - A Review," *https://doi.org/10.1177/096739111302100602*, vol. 21, no. 6, pp. 341–348, Jul. 2013, doi: 10.1177/096739111302100602.

[5] "Composite Definition & Meaning - Merriam-Webster." Accessed: Sep. 24, 2024. [Online]. Available: https://www.merriam-webster.com/dictionary/composite

[6] I. S. Abbood, S. A. Odaa, K. F. Hasan, and M. A. Jasim, "Properties evaluation of fiber reinforced polymers and their constituent materials used in structures – A review," *Mater Today Proc*, vol. 43, pp. 1003–1008, Jan. 2021, doi: 10.1016/J.MATPR.2020.07.636.

[7] S. Lampman *et al.*, Eds., *Fatigue and Fracture*, vol. 19. ASM International, 1996. doi: 10.31399/asm.hb.v19.9781627081931.

[8] Y. K. Lin, H. K. Liu, W. S. Kuo, and Y. Der Chen, “Fracture evolution in thick composites under compression,” *Polym Compos*, vol. 28, no. 4, pp. 425–436, Aug. 2007, doi: 10.1002/PC.20352.

[9] S. D. Müzel, E. P. Bonhin, N. M. Guimarães, and E. S. Guidi, “Application of the finite element method in the analysis of composite materials: A review,” Apr. 01, 2020, *MDPI AG*. doi: 10.3390/POLYM12040818.

[10] D. Dreese, “Correlation of a predictive analytical model to experimental results for a thick composite plate in a bolted joint configuration,” 2000. [Online]. Available: https://repository.rit.edu/theses

[11] N. Liu and W. Yu, “Evaluation of smeared properties approaches and mechanics of structure genome for analyzing composite beams,” *Mechanics of Advanced Materials and Structures*, vol. 25, no. 14, pp. 1171–1185, Oct. 2018, doi: 10.1080/15376494.2017.1330977.

[12] A. Gorjipoor, S. Van Hoa, and R. Ganesan, “Numerical model for investigation of the strain distribution in thick composite plates subjected to bolt loads,” *Aerosp Sci Technol*, vol. 59, pp. 94–102, Dec. 2016, doi: 10.1016/J.AST.2016.10.008.

[13] A. Gorjipoor, J. F. Simpson, R. Ganesan, and S. V. Hoa, “Computational and experimental strain analysis of flexural bending of thick glass/epoxy laminates,” *Compos Struct*, vol. 176, pp. 526–538, Sep. 2017, doi: 10.1016/J.COMPSTRUCT.2017.05.066.

[14] H. Hamidi, W. Xiong, S. V. Hoa, and R. Ganesan, “Fatigue behavior of thick composite laminates under flexural loading,” *Compos Struct*, vol. 200, pp. 277–289, Sep. 2018, doi: 10.1016/J.COMPSTRUCT.2018.05.149.

[15] S. Gul, I. E. Tabrizi, B. S. Okan, A. Kefal, and M. Yildiz, “An experimental investigation on damage mechanisms of thick hybrid composite structures under flexural loading using multi-instrument measurements,” *Aerosp Sci Technol*, vol. 117, p. 106921, Oct. 2021, doi: 10.1016/J.AST.2021.106921.

[16] P. J. Gray, R. M. O’Higgins, and C. T. McCarthy, “Effects of laminate thickness, tapering and missing fasteners on the mechanical behaviour of single-lap, multi-bolt, countersunk composite joints,” *Compos Struct*, vol. 107, no. 1, pp. 219–230, Jan. 2014, doi: 10.1016/J.COMPSTRUCT.2013.07.017.

[17] M. Bhong *et al.*, “Review of composite materials and applications,” *Mater Today Proc*, Oct. 2023, doi: 10.1016/J.MATPR.2023.10.026.

[18] J.-V. Poncelet, *Introduction à la mécanique industrielle, physique ou expérimentale*. 1841.

[19] A. Boresi and R. Schmidt, *Advanced Mechanics of Materials*, 6th ed. JohnWiley&Sons, 2002.

[20] A. Wöhler, “Wöhler’s experiments on the strength of metals,” *Engineering 4*, 1867.

[21] A. Vassilopoulos, Ed., *Fatigue Life Prediction of Composites and Composite Structures*, 2nd ed. Lausanne: Woodhead Publishing, 2020.

[22] A. Djabali, L. Toubal, R. Zitoune, and S. Rechak, “Fatigue damage evolution in thick composite laminates: Combination of X-ray tomography, acoustic emission and digital image correlation,” *Compos Sci Technol*, vol. 183, p. 107815, Oct. 2019, doi: 10.1016/J.COMPSCITECH.2019.107815.

[23] M. Makkonen, “Predicting the total fatigue life in metals,” *Int J Fatigue*, vol. 31, no. 7, pp. 1163–1175, Jul. 2009, doi: 10.1016/J.IJFATIGUE.2008.12.008.

[24] M. Kamal and M. M. Rahman, “Advances in fatigue life modeling: A review,” *Renewable and Sustainable Energy Reviews*, vol. 82, pp. 940–949, Feb. 2018, doi: 10.1016/J.RSER.2017.09.047.

[25] E. Narvydas, N. Puodziuniene, E. Narvydas, and N. Puodziuniene, “Applications of Sub-modeling in Structural Mechanics,” 2014, Accessed: Sep. 24, 2024. [Online]. Available: https://www.researchgate.net/publication/282611969

[26] A. Luís Gamino *et al.*, “Railway Infrastructure Asset Analysis Using A Global-Local Approach,” 2016, doi: 10.21012/FC11.092330.

[27] Z. Liu *et al.*, “Global-local fatigue assessment of an ancient riveted metallic bridge based on submodelling of the critical detail,” *Fatigue Fract Eng Mater Struct*, vol. 42, no. 2, pp. 546–560, Feb. 2019, doi: 10.1111/FFE.12930.

[28] A. E. Bogdanovich and I. Kizhakkethara, “Three-dimensional finite element analysis of double-lap composite adhesive bonded joint using submodeling approach,” *Compos B Eng*, vol. 30, no. 6, pp. 537–551, Sep. 1999, doi: 10.1016/S1359-8368(99)00026-8.

[29] A. Baker, *Composite Materials for Aircraft Structures*, Second. Blacksburg: American Institute of Aeronautics and Astronautics, Inc., 2004. Accessed: Apr. 20, 2024. [Online]. Available: https://books.google.com/books?id=5SPAIKFmFjcC

[30] A. Pramanik *et al.*, “Joining of carbon fibre reinforced polymer (CFRP) composites and aluminium alloys – A review,” *Compos Part A Appl Sci Manuf*, vol. 101, pp. 1–29, Oct. 2017, doi: 10.1016/J.COMPOSITESA.2017.06.007.

[31] K. P. Raju, K. Bodjona, G. H. Lim, and L. Lessard, “Improving load sharing in hybrid bonded/bolted composite joints using an interference-fit bolt,” *Compos Struct*, vol. 149, pp. 329–338, Aug. 2016, doi: 10.1016/J.COMPSTRUCT.2016.04.025.

[32] P. Zuo and A. P. Vassilopoulos, “Review of fatigue of bulk structural adhesives and thick adhesive joints,” *International Materials Reviews*, vol. 66, no. 5, pp. 313–338, Jul. 2021, doi: 10.1080/09506608.2020.1845110/ASSET/IMAGES/LARGE/10.1080_09506608.2020.1845110-FIG18.JPEG.

[33] J. Jakobsen, B. Endelt, and F. Shakibapour, “Bolted joint method for composite materials using a novel fiber/metal patch as hole reinforcement—Improving both static and fatigue properties,” *Compos B Eng*, vol. 269, p. 111105, Jan. 2024, doi: 10.1016/J.COMPOSITESB.2023.111105.

[34] L. Zhou, D. Zhang, L. Zhao, X. Zhou, J. Zhang, and F. Liu, “Design and analysis of a novel bolted composite π joint under bending load,” *Mater Des*, vol. 98, pp. 201–208, May 2016, doi: 10.1016/J.MATDES.2016.02.113.

[35] A. A. Pisano and P. Fuschi, “Mechanically fastened joints in composite laminates: Evaluation of load bearing capacity,” *Compos B Eng*, vol. 42, no. 4, pp. 949–961, Jun. 2011, doi: 10.1016/J.COMPOSITESB.2010.12.016.

[36] J. Hu, K. Zhang, Q. Yang, H. Cheng, P. Liu, and Y. Yang, “An experimental study on mechanical response of single-lap bolted CFRP composite interference-fit joints,” *Compos Struct*, vol. 196, pp. 76–88, Jul. 2018, doi: 10.1016/J.COMPSTRUCT.2018.05.016.

[37] P. P. Camanho, S. Bowron, and F. L. Matthews, “Failure Mechanisms in Bolted CFRP,” *http://dx.doi.org/10.1177/073168449801700302*, vol. 17, no. 3, pp. 205–233, Feb. 1998, doi: 10.1177/073168449801700302.

[38] D. Yoon, S. Kim, J. Kim, and Y. Doh, “Study on bearing strength and failure mode of a carbon-epoxy composite laminate for designing bolted joint structures,” *Compos Struct*, vol. 239, p. 112023, May 2020, doi: 10.1016/J.COMPSTRUCT.2020.112023.

[39] S. D. Thoppul, J. Finegan, and R. F. Gibson, “Mechanics of mechanically fastened joints in polymer–matrix composite structures – A review,” *Compos Sci Technol*, vol. 69, no. 3–4, pp. 301–329, Mar. 2009, doi: 10.1016/J.COMPSCITECH.2008.09.037.

[40] V. Mara, R. Haghani, and M. Al-Emrani, “Improving the performance of bolted joints in composite structures using metal inserts,” *http://dx.doi.org/10.1177/0021998315615204*, vol. 50, no. 21, pp. 3001–3018, Nov. 2015, doi: 10.1177/0021998315615204.

[41] HS Wang, CL Hung, and FK Chang, “Bearing Failure of bolted composite joints. Part 1: Experimental Characterization,” *J Compos Mater*, 1995.

[42] V. P. Lawlor, M. A. McCarthy, and W. F. Stanley, “An experimental study of bolt–hole clearance effects in double-lap, multi-bolt composite joints,” *Compos Struct*, vol. 71, no. 2, pp. 176–190, Nov. 2005, doi: 10.1016/J.COMPSTRUCT.2004.09.025.

[43] L. Liu, J. Zhang, K. Chen, and H. Wang, “Combined and interactive effects of interference fit and preloads on composite joints,” *Chinese Journal of Aeronautics*, vol. 27, no. 3, pp. 716–729, Jun. 2014, doi: 10.1016/J.CJA.2014.04.014.

[44] J. Hu, K. Zhang, Y. Xu, H. Cheng, G. Xu, and H. Li, “Modeling on bearing behavior and damage evolution of single-lap bolted composite interference-fit joints,” *Compos Struct*, vol. 212, pp. 452–464, Mar. 2019, doi: 10.1016/J.COMPSTRUCT.2019.01.044.

[45] C. T. McCarthy and P. J. Gray, “An analytical model for the prediction of load distribution in highly torqued multi-bolt composite joints,” *Compos Struct*, vol. 93, no. 2, pp. 287–298, Jan. 2011, doi: 10.1016/J.COMPSTRUCT.2010.09.017.

[46] Y. Cao, Z. Cao, Y. Zuo, L. Huo, J. Qiu, and D. Zuo, “Numerical and experimental investigation of fitting tolerance effects on damage and failure of CFRP/Ti double-lap single-bolt joints,” *Aerosp Sci Technol*, vol. 78, pp. 461–470, Jul. 2018, doi: 10.1016/j.ast.2018.04.042.

[47] T. N. Chakherlou, M. Mirzajanzadeh, and J. Vogwell, “Experimental and numerical investigations into the effect of an interference fit on the fatigue life of double shear lap joints,” *Eng Fail Anal*, vol. 16, no. 7, pp. 2066–2080, Oct. 2009, doi: 10.1016/J.ENGFAILANAL.2009.01.009.

[48] J. Wei, G. Jiao, P. Jia, and T. Huang, “The effect of interference fit size on the fatigue life of bolted joints in composite laminates,” *Compos B Eng*, vol. 53, pp. 62–68, Oct. 2013, doi: 10.1016/J.COMPOSITESB.2013.04.048.

[49] G. Kelly and S. Hallström, “Bearing strength of carbon fibre/epoxy laminates: Effects of bolt-hole clearance,” *Compos B Eng*, vol. 35, no. 4, pp. 331–343, 2004, doi: 10.1016/j.compositesb.2003.11.001.

[50] M. A. McCarthy, C. T. McCarthy, and G. S. Padhi, “A simple method for determining the effects of bolt–hole clearance on load distribution in single-column multi-bolt composite

joints," *Compos Struct*, vol. 73, no. 1, pp. 78–87, May 2006, doi: 10.1016/J.COMPSTRUCT.2005.01.028.

[51] R. T. Cole, E. J. Bateh, and J. Potter, "Fasteners for composite structures," *Composites*, vol. 13, no. 3, pp. 233–240, Jul. 1982, doi: 10.1016/0010-4361(82)90005-2.

[52] G. Xu, T. Gu, D. Zhao, and X. Li, "Modeling on displacement response and damage mechanism of contact interface during installation for composites sleeved interference joint," *Compos Struct*, vol. 316, p. 117025, Jul. 2023, doi: 10.1016/J.COMPSTRUCT.2023.117025.

[53] R. T. Cole and E. J. Bateh, "Special Fastener Development For Composite Structure," 1982.

[54] G. Xu *et al.*, "Modeling of damage behavior of carbon fiber reinforced plastic composites interference bolting with sleeve," *Mater Des*, vol. 194, p. 108904, Sep. 2020, doi: 10.1016/J.MATDES.2020.108904.

[55] G. Xu *et al.*, "An experimental study on mechanical behavior and failure mechanism of sleeved fasteners and conventional bolt for composite interference-fit joints," *Thin-Walled Structures*, vol. 170, Jan. 2022, doi: 10.1016/j.tws.2021.108537.

[56] D. Falconieri and F. Franco, "The effect of titanium insert repairs on the static strength of CFRP coupons and joints," *Compos Struct*, vol. 134, pp. 799–810, Dec. 2015, doi: 10.1016/J.COMPSTRUCT.2015.08.042.

[57] Y. Fu, E. Ge, H. Su, J. Xu, and R. Li, "Cold expansion technology of connection holes in aircraft structures: A review and prospect," *Chinese Journal of Aeronautics*, vol. 28, no. 4, pp. 961–973, Aug. 2015, doi: 10.1016/J.CJA.2015.05.006.

[58] B. Ferret, M. Anduze, and C. Nardari, “Metal inserts in structural composite materials manufactured by RTM,” *Compos Part A Appl Sci Manuf*, vol. 29, no. 5–6, pp. 693–700, Jan. 1998, doi: 10.1016/S1359-835X(97)00107-3.

[59] J. Troschitz, R. Kupfer, and M. Gude, “Process-integrated embedding of metal inserts in continuous fibre reinforced thermoplastics,” *Procedia CIRP*, vol. 85, pp. 84–89, Jan. 2019, doi: 10.1016/J.PROCIR.2019.09.039.

[60] M. Ridha, Z. Su, L. Q. N. Tran, W. M. A. Yek, S. Narayanaswamy, and T. E. Tay, “Effect of geometry and adhesion on the performance of fiber reinforced thermoplastic composite joints with metal inserts,” *Compos Part A Appl Sci Manuf*, vol. 187, p. 108482, Dec. 2024, doi: 10.1016/J.COMPOSITESA.2024.108482.

[61] J. Gebhardt and J. Fleischer, “Experimental Investigation and Performance Enhancement of Inserts in Composite Parts,” *Procedia CIRP*, vol. 23, no. C, pp. 7–12, Jan. 2014, doi: 10.1016/J.PROCIR.2014.10.084.

[62] M. A. Shaheen, A. Alsaleh, and L. S. Cunningham, “Experimental tests on a novel bolt sleeve device to increase the ductility of steel end plate connections,” *J Constr Steel Res*, vol. 214, p. 108510, Mar. 2024, doi: 10.1016/J.JCSR.2024.108510.

[63] “User Assistance R2023x, Simulation, Structures: Abaqus,” DassaultSystemes.

[64] R. Budynas and K. Nisbett, *Shigley’s Mechanical Engineering Design*, 9th ed. McGraw-Hill, 2011.

[65] L. V. Awadhani and A. Bewoor, “Parametric study of composite bolted joint under compressive loading,” *Procedia Manuf*, vol. 22, pp. 186–195, Jan. 2018, doi: 10.1016/J.PROMFG.2018.03.029.

[66] B. Okutan, “The effects of geometric parameters on the failure strength for pin-loaded multi-directional fiber-glass reinforced epoxy laminate,” Turkey, 2003. [Online]. Available: www.elsevier.com/locate/compositesb

[67] A. Elkady, “ABAQUS Tutorial: Creating a Submodel,” Youtube.com. Accessed: Oct. 11, 2024. [Online]. Available: https://www.youtube.com/watch?v=Y3dGw32NztM